HHS Public Access

Author manuscript

Sci Transl Med. Author manuscript; available in PMC 2016 May 24.

Published in final edited form as:

Sci Transl Med. 2016 April 6; 8(333): 333ra50. doi:10.1126/scitranslmed.aad6100.

Cyclodextrin promotes atherosclerosis regression via macrophage reprogramming

Sebastian Zimmer[1,†], **Alena Grebe**[2,†], **Siril S. Bakke**[2,3,16], **Niklas Bode**[1], **Bente Halvorsen**[4], **Thomas Ulas**[5], **Mona Skjelland**[6], **Dominic De Nardo**[2,7], **Larisa I. Labzin**[2], **Anja Kerksiek**[8], **Chris Hempel**[9], **Michael T. Heneka**[10], **Victoria Hawxhurst**[11], **Michael L Fitzgerald**[11], **Jonel Trebicka**[12], **Jan-Åke Gustafsson**[13], **Marit Westerterp**[14], **Alan R. Tall**[14], **Samuel D. Wright**[15], **Terje Espevik**[3], **Joachim L. Schultze**[5], **Georg Nickenig**[1], **Dieter Lütjohann**[8], and **Eicke Latz**[2,3,16,17,*]

[1]Medizinische Klinik und Poliklinik II, University Hospitals Bonn, 53105 Bonn, Germany

[2]Institute of Innate Immunity, University Hospitals Bonn, 53127 Bonn, Germany

[3]Centre of Molecular Inflammation Research at the Norwegian University of Science and Technology, 7489 Trondheim, Norway

[4]Research Institute of Internal Medicine, Oslo University Hospital Rikshospitalet, Norway; Institute of Clinical Medicine and K.G. Jebsen Inflammatory Research Center, University of Oslo, 0424 Oslo, Norway

[5]Genomics and Immunoregulation, Life and Medical Sciences Institute, University of Bonn, 53115 Bonn, Germany

[6]Department of Neurology, Oslo University Hospital and University of Oslo, Oslo, Norway

[7]Inflammation Division, The Walter and Eliza Hall Institute of Medical Research, Parkville Victoria 3052, Australia

[8]Institute of Clinical Chemistry und Clinical Pharmacology, University Hospitals Bonn, 53105 Bonn, Germany

[9]Addi and Cassi Fund, Reno, NV 89511, USA

[10]Clinic and Polyclinic for Neurology, University Hospitals Bonn, 53105 Bonn, Germany

[11]Lipid Metabolism Unit, Center for Computational and Integrative Biology, Boston, MA 02114, USA

[*]To whom correspondence should be addressed: Eicke Latz, MD, PhD, Institute of Innate Immunity, University Hospitals Bonn, Sigmund-Freud-Str. 25, 53127 Bonn, Germany, ; Email: eicke.latz@uni-bonn.de, phone: +49 228 287 51223

[†]equal contribution

Author contributions: S.Z., A.G. designed, performed and analyzed experiments. N.B. assisted with atherosclerosis mouse models and data analysis. S.S.B., L.I.L., B.H., M.S. A.K. and V.H. performed experiments. S.S.B., T.U. and J.L.S. performed bioinformatic analyses. J.A.G., M.T.H., M.W. and A.R.T. provided knock-out mice. D.D., G.N., T.E., M.L.F., S.D.W., and D.L. analyzed data and provided critical suggestions and discussions throughout the study. C.H. provided the initial idea for the study. S.Z., A.G. and E.L. designed the study and wrote the manuscript.

Competing interests: No relevant competing interests.

Data and materials availability: Accession codes are available in Gene Expression Omnibus (GEO): GSE67014 (includes GSE67011 and GSE67013)

[12]Medizinische Klinik und Poliklinik I, University Hospitals Bonn, 53105 Bonn, Germany

[13]Center for Nuclear Receptors and Cell Signaling, University of Houston, Houston, TX 77004, USA

[14]Department of Medicine, Columbia University, New York, NY 10032, USA

[15]CSL Behring, King of Prussia, PA 19406, USA

[16]Department of Infectious Diseases and Immunology, UMass Medical School, Worcester, MA 01605, USA

[17]German Center of Neurodegenerative Diseases (DZNE), 53127 Bonn, Germany

Abstract

Atherosclerosis is an inflammatory disease linked to elevated blood cholesterol levels. Despite ongoing advances in the prevention and treatment of atherosclerosis, cardiovascular disease remains the leading cause of death worldwide. Continuous retention of apolipoprotein B-containing lipoproteins in the subendothelial space causes a local overabundance of free cholesterol. Since cholesterol accumulation and deposition of cholesterol crystals (CCs) triggers a complex inflammatory response, we tested the efficacy of the cyclic oligosaccharide 2-hydroxypropyl-β-cyclodextrin (CD), a compound that increases cholesterol solubility, in preventing and reversing atherosclerosis. Here we show that CD treatment of murine atherosclerosis reduced atherosclerotic plaque size and CC load, and promoted plaque regression even with a continued cholesterol-rich diet. Mechanistically, CD increased oxysterol production in both macrophages and human atherosclerotic plaques, and promoted liver X receptor (LXR)-mediated transcriptional reprogramming to improve cholesterol efflux and exert anti-inflammatory effects. *In vivo*, this CD-mediated LXR agonism was required for the anti-atherosclerotic and anti-inflammatory effects of CD as well as for augmented reverse cholesterol transport. Since CD treatment in humans is safe and CD beneficially affects key mechanisms of atherogenesis, it may therefore be used clinically to prevent or treat human atherosclerosis.

Introduction

Atherosclerosis is the underlying pathology that causes heart attack, stroke and peripheral vascular disease. Collectively, these conditions represent a common health problem and current treatments are insufficient to adequately reduce the risk of disease development. Pharmacologic reduction (1–3) of high cholesterol levels is among the most successful therapeutic approaches to reduce the risk of developing cardiovascular disease and stroke but adequate reduction of low-density lipoprotein cholesterol is not possible in all patients.

Atherosclerosis is characterized by arterial wall remodeling which is initiated by the retention and accumulation of different classes of lipids in the subendothelial layer. Lipid deposition and the appearance of cholesterol crystals (CCs) has been associated with the induction of an inflammatory reaction in the vessel wall, which contributes to the pathogenesis (4, 5). Indeed, patients with increased systemic inflammation have increased risk of cardiovascular death and studies are underway that test whether anti-inflammatory treatment can reduce cardiovascular event rates (6).

CCs which can result from excessive cholesterol deposition in atherosclerotic lesions, are among the proinflammatory triggers that contribute to the inflammatory response during atherogenesis (7). CCs can trigger complement activation, neutrophil net formation as well as induction of innate immune pathways (4, 5, 8–10). Hence, therapeutic strategies aimed at the prevention of cholesterol phase transition or the removal of CCs could reduce tissue inflammation and disease progression.

Genetic approaches to increase the capacity of macrophages to remove free cholesterol from atherosclerotic lesions have proven to be highly successful in preclinical trials (11). This prompted us to test whether pharmacologically increasing cholesterol solubility, clearance and catabolism can be exploited for the prevention or treatment of atherosclerosis. 2-hydroxypropyl-β-cyclodextrin (CD) is an FDA-approved substance used to solubilize and entrap numerous lipophilic pharmaceutical agents for therapeutic delivery in humans (12, 13). While it has previously been shown that CD increases cholesterol solubility, promotes the removal of cholesterol from foam cells *in vitro* and initiates anti-inflammatory mechanisms (14–16), it remains unknown whether CD can exert anti-atherogenic effects *in vivo*.

Here, we found that subcutaneous administration of CD profoundly reduced atherogenesis and induced regression of established atherosclerosis. CD augmented cholesterol metabolism from CCs leading to their reduced appearance in lesions. Furthermore, CD increased cholesterol metabolism and liver X receptor (LXR)-dependent cellular reprogramming, which resulted in more efficient reverse cholesterol transport (RCT) as well as reduced pro-inflammatory gene expression. The atheroprotective effect of CD was dependent on LXR expression in myeloid cells when transplanted in LDLR deficient mice. These studies suggest that CD mediates atheroprotection via increased production of oxysterols and LXR dependent cellular reprogramming and provide preclinical evidence that CD could be developed into an effective therapy of atherosclerosis in humans.

Results

Cyclodextrin treatment impairs atherogenesis

To investigate the efficacy of CD treatment in murine atherosclerosis, ApoE$^{-/-}$ mice were fed a cholesterol-rich diet and concomitantly treated subcutaneously with CD or vehicle control for eight weeks. While plasma cholesterol, the main driver of atherosclerosis, remained unaffected (Fig. 1A), CD treatment profoundly reduced atherosclerotic lesions within the aortic root (Fig. 1B). Furthermore, we found reduced amounts of CCs in atherosclerotic plaques of CD treated mice as assessed by laser reflection microscopy (Fig. 1C, D). CD did not influence weight gain, blood pressure, heart rate or the number of bone marrow-derived or circulating sca1/flk1 positive cells (Fig. S1A–E). Moreover, plasma levels of phytosterols, cholestanol and cholesterol precursors were not influenced by CD treatment, indirectly showing that CD did not alter cholesterol enteric uptake or overall endogenous biosynthesis (Fig. S1F) (17). CD also did not change the relative plaque composition, including cellularity and macrophage content (Fig. 1E, F). However, production of aortic reactive oxygen species (Fig. 1G) and plasma levels of pro-

inflammatory cytokines were reduced by CD treatment (Fig. 1H–J), suggesting that CD may reduce the inflammatory response during atherogenesis.

Cyclodextrin treatment mediates regression of atherosclerotic plaques

Although continuous drug administration in parallel to Western diet feeding of mice is a standard protocol to investigate potential atheroprotective substances (18), patients are generally not treated in early stages of atherogenesis. Therefore, we tested the effect of CD treatment on atherosclerosis regression. ApoE$^{-/-}$ mice are hypercholesterolemic even under normal or lipid-reduced chow, and thus most murine atherosclerotic regression models rely on interventional strategies that normalize plasma lipids, such as viral gene transfer, transplantation or infusion of high-density lipoprotein (HDL) particles (19). We adapted a less invasive regression protocol (20), in which ApoE$^{-/-}$ mice were first fed a cholesterol-rich diet for eight weeks to induce advanced atherosclerotic lesions, and then switched to a normal chow diet for another four weeks, during which CD or vehicle control was administered (Fig. 2A). As expected, plasma cholesterol concentrations were decreased in both groups compared to pretreatment, but no difference between control and CD treatment was observed (Fig. 2B, Fig. S2A). While switching to a normal chow diet had no effect on atherosclerotic lesion size in vehicle treated mice, CD treatment resulted in a regression of atherosclerotic plaques by approximately 45% (Fig. 2C).

Although CC load in lesions was already decreased in vehicle treated animals compared to pretreatment, CC amounts were further reduced by CD treatment (Fig. 2D). Because patients with cardiovascular disease often do not adhere to the recommended lifestyle changes, which include dietary modifications, we next investigated whether CD treatment can affect atherosclerosis regression during continuous enteric cholesterol challenge. CD or vehicle treatment was started after eight weeks of cholesterol-rich diet, which was continued for the entire 12 weeks (Fig. 2E). While plasma cholesterol and general cholesterol metabolism were not altered (Fig. 2F, Fig. S2B), atherosclerotic plaque size and CC load were decreased in CD treated mice on continuous cholesterol-rich diet (Fig. 2G, H). These data demonstrate that CD treatment is efficient in reducing established plaques.

Cyclodextrin dissolves extra- and intracellular cholesterol crystals

There are several possibilities to explain the protective effects of CD treatment on both atherogenesis and established atherosclerosis. Since CD is known to form soluble inclusion complexes with cholesterol, thereby enhancing its solubility in aqueous solutions by approximately 150,000-fold, we tested whether CD increases the solubility of CCs. Indeed, fluorescent CD bound to the surface of CCs (Fig. 3A, B) and CD mediated the solubilization of CCs in a dose-dependent manner (Fig. 3C). To be effective in atherosclerotic plaques, CD must also act on intracellular CCs. Indeed, macrophages rapidly internalized fluorescent CD (Fig. 3D) and concentrated it in intracellular compartments (Fig. 3E). Furthermore, incubation with 10 mM CD, a subtoxic dose (Fig. S3), enhanced the dissolution of intracellular CCs over time (Fig. 3F, Fig. S4).

Metabolism of crystal-derived cholesterol is increased by cyclodextrin

Macrophages within the arterial wall take up excessive amounts of cholesterol and transform into foam cells, a process that can impair macrophage function and promote atherogenesis (21). This can be mimicked *in vitro* by loading macrophages with CCs (Fig. S5). After uptake of CCs into phagosomes, cholesterol is moved from the lysosome via the Niemann-Pick C1 (NPC1) transporter to the endoplasmic reticulum where acetyl-CoA acetyltransferase catalyzes the formation of cholesteryl esters. This mechanism turns excess free cholesterol, which forms crystals and is cytotoxic, into cholesteryl esters that can be stored in lipid droplets. A second pathway to metabolize free cholesterol is the formation of water-soluble oxysterols. Oxysterols can diffuse across cell membranes and are known to reprogram macrophages via activation of LXR, which in turn modulates the inflammatory response and supports RCT to HDL (22–24). To study how CD influences the ability of macrophages to reduce the amount of cholesterol derived from CCs, we incubated macrophages with CCs prepared from D_6-cholesterol (D_6-CCs) and followed D_6-cholesterol metabolism products in cells and cellular supernatants by gas chromatography-mass spectrometry selective ion monitoring (GC-MS-SIM) (Fig. 4A). This analysis revealed that CD treatment promoted esterification of crystal-derived D_6-cholesterol (Fig. 4B). Furthermore, CD amplified D_6-cholesterol concentrations in supernatants, while reducing the overall cellular pool of D_6-cholesterol (Fig. 4C). Hence, CD treatment increased the cholesterol efflux capacity of macrophages, which represents an important protective factor in patients with coronary artery disease (25, 26). Active cholesterol transport is mediated primarily by the ATP-binding cassette transporters A1 and G1 (ABCA1 and ABCG1), which transfer free cholesterol to ApoA1 and mature HDL particles, respectively (27). In line with the observed increase in cholesterol efflux capacity, macrophages incubated with CCs had increased expression of both ABCA1 and ABCG1, which was even further enhanced by CD treatment (Fig. 4D–F). Genes involved in driving cholesterol efflux, including *Abca1* and *Abcg1*, are under control of the liver X receptor/ retinoid X receptor (LXR/RXR) transcription apparatus (22, 28). Since the transcriptional activities of LXRs are positively regulated by oxysterols, we next analyzed whether CD can potentiate cholesterol oxidation. Indeed, we found that CD treatment of D_6-CCs loaded macrophages led to a dramatic 15-fold increase of D_6-cholesterol-derived 27-hydroxycholesterol (D_5-27-hydroxycholesterol) (Fig. 4G). Unexpectedly, CD also significantly increased 27-hydroxycholesterol production and secretion from macrophages under normocholesterolemic conditions, meaning macrophages not treated with D_6-CCs (Fig. 4H). Hence, CD leads to increased metabolism of free cholesterol and could thereby lower the potential for its phase transition into crystals.

Cyclodextrin induces LXR target gene expression in macrophages

The drastic CD-mediated increase of oxysterol production upon D_6-CC loading and the unanticipated finding that CD can increase oxysterols in normocholesterolemic macrophages prompted us to comprehensively investigate whether CD influences the expression profiles of LXR-regulated genes. Wild type (WT) or LXR$\alpha^{-/-}\beta^{-/-}$ macrophages were exposed to CD, CC or CC and CD, and gene expression was assessed by genome-wide mRNA profiling. To investigate whether CD changes LXR target gene expression in macrophages, we performed gene set enrichment analysis (GSEA) (29) with a set of 533 of previously identified LXR target genes (30) (Fig. 5A and Table S1). Enrichment of LXR target gene

sets was identified when WT macrophages were incubated with CCs (Fig. 5B), presumably due to cholesterol overloading of macrophages. Consistent with the strong induction of CC-derived 27-hydroxycholesterol and the observed increase in cholesterol efflux by CD, LXR target gene sets were enriched when CD was added together with CCs (Fig. 5B). CD treatment alone also led to LXR gene set enrichment under normocholesterolemic conditions, which correlates to the observed induction of cellular 27-hydroxycholesterol (Fig. 4H). In LXR$\alpha^{-/-}\beta^{-/-}$ macrophages none of the conditions resulted in significant enrichments of LXR target gene sets (Fig. 5C). Furthermore, these findings could be confirmed for the key LXR target genes ABCA1 and ABCG1 in WT and LXR$\alpha^{-/-}\beta^{-/-}$ macrophages on mRNA and protein levels (Fig. 5D–F) (31).

Cyclodextrin increases in vivo reverse cholesterol transport

To test whether CD-induced LXR-reprogramming of macrophages improves macrophage cholesterol efflux *in vivo*, bone marrow-derived macrophages (BMDM) from WT or LXR$\alpha^{-/-}\beta^{-/-}$ mice were loaded with D_6-CCs *ex vivo* and injected into the peritoneum of WT mice. The mice carrying crystal-loaded macrophages were then treated with CD or vehicle control and D_6-cholesterol excretion into the feces and urine was monitored by GC-MS-SIM (Fig. 6A). CD increased RCT of crystal-derived D_6-cholesterol from WT, and to a lower extent from LXR$\alpha^{-/-}\beta^{-/-}$ macrophages (Fig. 6B). Of note, CD treatment not only induced D_6-cholesterol excretion into the feces but also promoted urinary D_6-cholesterol elimination (Fig. 6C), a process that is normally not observed during RCT. Prior work on Niemann-Pick type C disease, a rare genetic disorder in which cholesterol cannot escape the lysosome, has shown that CD can mobilize lysosomal cholesterol and activate LXR-dependent gene expression (32, 33). NPC1-deficient patients receive weekly injections of CD with the aim of overcoming this cholesterol transport defect (ClinicalTrial.gov NCT01747135). To investigate whether CD can also lead to urinary cholesterol excretion in humans, we monitored urinary cholesterol excretion of patients with NPC1 mutations after CD infusion over time. Indeed, CD, which is primarily excreted via the urinary tract, led to a time-dependent cholesterol excretion into the urine (Fig. 6D). These data suggest that CD enhances *in vivo* RCT from macrophages, partially in an LXR-dependent manner, but can also directly extract and transport cholesterol for excretion.

Cyclodextrin modifies human plaque cholesterol metabolism and gene expression

To test whether the protective functions of CD on murine macrophages are also exerted in human atherosclerotic plaques, we next performed lipid and genomic analyses on biopsy specimens obtained from carotid endarterectomies (Fig. 7A). Comparable to our findings in murine macrophages, incubation of human atherosclerotic plaques with CD resulted in a transfer of cholesterol from plaques to supernatants (Fig. 7B). Moreover, we observed an increase in the production of 27-hydroxycholesterol, which was mainly released into the supernatants of the CD treated plaques (Fig. 7C). Gene expression profiling of a large panel of human immunology-related genes and selected LXR target genes was performed in resting or treated plaque tissue. This gene expression data was analyzed using several bioinformatics approaches. First, we performed gene ontology enrichment analysis (GOEA) using the genes differentially regulated after treatment with CD or vehicle control. Consistent with our lipid results, we found that genes involved in lipid transport, storage,

metabolism and efflux were up-regulated upon CD exposure. Conversely, genes known to regulate immune responses, represented by terms such as ‘regulation of immune responses in lymphocytes’, ‘regulation of leukocyte mediated immunity’ or ‘interleukin response, T cell and NK cell regulation’ were down-regulated after CD treatment (Fig. 7D). Further interrogation of the GOEA revealed that CD treatment of human plaques affected many key genes in the GO term “regulation of inflammatory response” (GO:0050727). These included innate immune receptors, such as TLRs 2, 3, 4, 7 and 9, the TLR adapter MyD88 as well as the inflammasome sensor NLRP3 and the inflammasome-dependent pro-inflammatory cytokines IL-1β and IL-18 (Fig. 7E). Since we observed that CD increased the endogenous LXR agonist 27-hydroxycholesterol, we next analyzed whether CD regulates the expression of LXR target genes in human atherosclerotic plaques. Indeed, GSEA revealed an enrichment of LXR target genes after CD treatment when compared to control treated plaques (Fig. 7F, Table S3). Additionally, many LXR target genes were found among the most differentially regulated genes (Fig. 7G red or blue gene labels). Of note, the inflammasome sensor *NLRP3* and the inflammasome inhibitor *HSP90AA1* (34) are both LXR target genes (24) and CD treatment resulted in *NLRP3* down-regulation and an up-regulation of *HSP90AA1* when compared to control (Fig. 7H). Together these data show that CD activates LXR dependent transcriptional programs in human plaques, influencing both cholesterol transport and several inflammatory processes, which are known to be relevant to the pathogenesis of atherosclerosis.

Atheroprotection by cyclodextrin is LXR dependent

We next tested whether the CD-mediated effects in isolated macrophages *in vitro* or in *ex vivo* treated human plaque material reflect the atheroprotective effects of CD in mice. As CD treatment lowered the systemic levels of LXR-modulated cytokines (IL-1β, IL-6 and TNF-α) (Fig. 1H–J) and also resulted in increased *Abca1* and *Abcg1* mRNA in the aortic arches of ApoE$^{-/-}$ mice fed a cholesterol-rich diet (Fig. S6) we determined whether CD-mediated atheroprotection *in vivo* requires LXR activation and cholesterol efflux via ABCA1 and ABCG1. We therefore transplanted WT, LXRα$^{-/-}$β$^{-/-}$ or MAC-ABC^{DKO} (LysmCreAbca1$^{fl/fl}$Abcg1$^{fl/fl}$) bone marrow into irradiated LDLR$^{-/-}$ mice. After bone marrow engraftment, the transplanted mice were fed a cholesterol-rich diet and were concomitantly treated with CD or vehicle control for eight weeks. CD treatment did not influence plasma cholesterol levels in the different transplant groups (Fig. 8A–C). The lipoprotein profiles also remained unchanged except that CD treatment slightly decreased the amount of HDL in LDLR$^{-/-}$ mice transplanted with MAC-ABC^{DKO} bone marrow (Fig. S7). LDLR$^{-/-}$ mice carrying WT bone marrow showed reduced atherosclerotic plaque size demonstrating that CD is also effective in the LDLR$^{-/-}$ model of atherosclerosis (Fig. 8D). Of note, CD treatment did not influence lesion development in LDLR$^{-/-}$ mice carrying LXRα$^{-/-}$β$^{-/-}$ bone marrow, highlighting that LXR agonism is critical for CD-mediated atheroprotection (Fig. 8E). In contrast, deficiency of ABCA1 and ABCG1 in macrophages did not influence the effectiveness of CD treatment (Fig. 8F), suggesting that CD can bypass these cholesterol efflux pathways.

To better understand how CD-dependent LXR agonism can ameliorate atherosclerosis we performed a genome-wide gene expression analysis from aortic tissue of LDLR$^{-/-}$ mice

transplanted with WT or LXR$\alpha^{-/-}\beta^{-/-}$ bone marrow. GOEA of differentially expressed genes demonstrated that important pathways involved in atherogenesis including lipid metabolism and inflammation were regulated by CD treatment in an LXR-dependent manner (Fig. 8G). Similar to our studies on human plaques, LXR target genes were found among the top differentially regulated genes upon CD treatment (Fig. 8H). Moreover, we confirmed our observations in human plaques that CD promoted up-regulation of the NLRP3 inhibitor *Hsp90aa1* and down-regulation of NLRP3 inflammasome genes in an LXR-dependent manner (Fig. 8I). Together these data suggest that the CD-mediated atheroprotection observed in murine atherosclerosis is dependent on LXR activation and that CD exerts multiple anti-inflammatory effects in atherosclerotic plaques.

Discussion

In this study we tested the hypothesis that increasing the solubility of cholesterol by pharmacological means can have beneficial effects on diet-induced atherosclerosis. The large effect observed and the unexpected ability of CD to promote regression of established atherosclerosis even under the extreme hypercholesterolemic conditions observed during a cholesterol-rich diet cannot be explained by simple mass action of CD alone. The results from the lipid and genomic discovery approaches combined with *in vivo* studies utilizing gene-deficient mice suggest that CD exerts its potent effect mainly by reprogramming cells in atherosclerotic plaques. By increasing the amount of endogenous LXR ligands, CD acts akin to a pro-drug except that it is not metabolized itself but rather promotes the metabolism of its cargo cholesterol into pharmacologically active metabolites.

It appears that transitory changes in cholesterol metabolism and inflammatory pathways are linked and that the activity of LXR is a key rheostat in this system. For example, innate immune activation by microbial components or the acute phase response can suppress expression of LXR target genes, such as ABCA1 and ABCG1, leading to cholesterol retention, which can augment an inflammatory reaction in various ways (35, 36). Indeed, it is conceivable that this type of innate immune amplification could be part of an evolutionarily conserved antimicrobial defense mechanism (23). The resulting cholesterol accumulation leads to an increase in LXR agonists, which in turn can counterbalance the inflammatory response and increase cholesterol efflux leading to restoration of cholesterol and immune homeostasis. However, due to the overabundance of pro-inflammatory dietary factors and an excess of cholesterol, this balance may be shifted towards chronic inflammation and cholesterol retention, which drive atherogenesis. By promoting cholesterol solubility, enhancing LXR activity and mobilizing cholesterol efflux, CD could therefore normalize both cholesterol and immune homeostasis in the vasculature.

The activity of CD on macrophages resembles that of the anti-atherogenic factor HDL. HDL relieves cells from excess cholesterol via ABC transporters and, in addition, our recent work shows that HDL can have dramatic anti-inflammatory effects on macrophages (37). However, HDL does not activate LXR but leads to increased expression of Activating Transcription Factor (ATF) 3, a key repressor of innate immune pathways (37). In contrast, while CD has the ability to increase HDL-mediated RCT it can additionally mobilize cholesterol for direct excretion into the urine and feces. These data suggest that CD can

bypass ABCA1- and ABCG1-mediated active cholesterol efflux. Consistent with these observations, our bone marrow transplantation studies indicate that the atheroprotective effects of CD are independent of the active cholesterol efflux process mediated by ABCA1 and ABCG1. This is in line with our recent findings demonstrating that synthetic LXR agonists mediate atheroprotection independent of macrophage ABCA1 and ABCG1 (38).

There are several limitations to our study. First, although our data demonstrate that CD promotes LXR activation in plaque macrophages and that LXR is required in myeloid cells for CD-mediated atheroprotection, we cannot exclude other unidentified pathways. Indeed, it is likely that CD-mediated atheroprotection is multifactorial and that the differential effects of CD such as physically increasing cholesterol solubility, promoting cholesterol metabolism and efflux in macrophages as well as its anti-inflammatory properties cannot easily be isolated. Second, although our data identified 27-hydroxycholesterol as the primary LXR-agonist upon CD treatment, other endogenous oxysterols may also contribute to LXR activation. In this context, functional activity of regulatory enzymes such as Cyp27A1 and differential effects in specific cell types would be interesting. Third, although our *ex vivo* experiments with carotid artery plaques suggest that CD can induce atheroprotective pathways in human disease, specific clinical trials are necessary to validate these findings.

Although preclinical models showing the effectiveness of LXR agonism in preventing murine atherosclerosis (39) and promoting atherosclerosis regression (40) provided promising prospects for clinical use of LXR agonists in atherosclerosis treatment, the progression of therapeutic molecules into the clinic was hampered by liver toxicity and lipogenic effects (41). CD on the other hand is already in clinical use in humans for the delivery of lipophilic drugs and has not shown relevant toxicity. Hence repurposing CD for the treatment or prevention of atherosclerosis would be feasible. Our studies provide a proof-of-principle that therapies aimed at increasing the solubility and removal of macrophage cholesterol could be an effective strategy for the treatment of atherosclerosis.

Materials and methods

Study design

The main objective of our study was to investigate whether CD exhibits atheroprotective effects and to identify the main mechanisms by which they are mediated. For this, we utilized murine models of atherosclerosis, studied macrophage biology *in vitro* and performed *ex vivo* experiments with human atherosclerotic plaques. Specific details of the individual experiments are described below.

ApoE$^{-/-}$ atherosclerosis mouse models

12-week old ApoE$^{-/-}$ mice (Charles River) on a C57BL/6J background were used for all studies. Animals were maintained in a 22 °C room with a 12 h light/dark cycle and received chow and drinking water ad libitum.

CD prevention protocol—ApoE$^{-/-}$ mice were fed a modified cholesterol-rich diet containing 21 % fat, 19.5 % casein, and 1.25 % cholesterol for 8 weeks (Ssniff, Soest). The

mice were subcutaneously injected with 2 g CD/ kg body weight or 200 μl 0.9 % NaCl as vehicle control twice a week.

CD regression protocol—ApoE$^{-/-}$ mice were first fed a cholesterol-rich diet for 8 weeks so that advanced atherosclerotic lesions could develop. The diet was then switched to normal chow for another 4 weeks. The mice were concomitantly treated with either CD or 200 μl 0.9 % NaCl as vehicle control as described above.

CD treatment protocol—ApoE$^{-/-}$ mice were fed a cholesterol-rich diet for a total of 12 weeks. CD or vehicle control treatment was started after 8 weeks as described above.

Body weights were measured weekly. Arterial blood pressure and heart rate were assessed with a computerized tail-cuff method (CODA 6, Kent Scientific) before and after treatment. The mice were sacrificed by cervical dislocation after the indicated treatments and tissue samples and blood were collected immediately. All animal experiments were performed in accordance with institutional guidelines and the German animal protection law.

Bone marrow transplantation model

Bone marrow was obtained from 14–18 week old donor mice: WT C57BL/6J, LXRα$^{-/-}$β$^{-/-}$ (mixed genetic background on C57BL/6J and 129/Sv strains) and MAC-ABC^{DKO} (LysmCreAbca1fl/flAbcg1fl/fl on C57BL/6J background). Donor bone marrow was collected by flushing femurs and tibiae with DMEM cell culture medium using a 23G needle. The suspension was filtered with a sterile 70μm nylon cell strainer and the cells subsequently washed twice with Hank's acid citrate dextrose solution and resuspended in PBS. For full engraftment of donor bone marrow, recipient LDLR$^{-/-}$ mice on a C57BL/6J background were subjected to lethal irradiation with 6×6 Gy over 4 h from a OB 29/4 (Cs-137). 4 h after irradiation, 1×10^7 cells from donor mice were injected intravenously via a tail vein. All mice received drinking water spiked with Ciprofloxacin 0.1 mg/ml for seven days to prevent systemic infection during neutropenia. The atherosclerosis trials were initiated four weeks after irradiation. All mice were fed a cholesterol-rich diet and concomitantly treated with CD or vehicle control for eight weeks as described above.

Histological analysis of murine atherosclerotic plaques

Hearts with ascending aortas were embedded in Tissue Tek OCT embedding medium (Miles), snap-frozen, and stored at −80°C. Samples were sectioned on a Leica cryostat (5 μm), starting at the aortic arch and progressing through the aortic valve area into the heart, and were placed on slides. For the detection of atherosclerotic lesions, aortic cryosections were fixed with 3.7% formaldehyde for 1 h, rinsed with deionised water, stained with Oil Red O working solution (0.5%) for 30 min, and were rinsed again. Hematoxylin staining was performed according to standard protocols. All sections were examined under a Zeiss Axiovert 200M microscope using AxioVision software. For quantification of atherosclerotic plaque formation in the aortic root, lesion area and total area of 3–4 serial histological sections of the aortic root were quantified per mouse. Atherosclerosis data are expressed as plaque area in percent of total vessel wall area. For analysis of cholesterol crystal plaque load, aortic cryosections were fixed with 4% paraformaldehyde for 30 min at 21°C. They

were then blocked and permeabilized with 5% fetal calf serum, 5% bovine serum albumin, 10% normal goat serum, 0.1% saponin in PBS for 60 min at 21°C. The primary rat anti-mouse CD68 antibody (MCA1957, AbD Serotec) was diluted to 2 μg/ml in 10% normal goat serum/ PBS and the slides were incubated overnight at 4°C. The secondary goat anti-rat IgG Alexa647 conjugate (Invitrogen) was diluted to 4 μg/ml in 10% normal goat serum/ PBS and the slides were incubated for 60 min in the dark at 21°C. The sections were again washed 3x with 10% normal goat serum/ PBS and subsequently counterstained with Hoechst 33342 (Immunochemistry) diluted to 5 μg/ml in PBS for 2 min in the dark at 21°C. Coverslips were mounted with 80% glycerol and the edges carefully sealed using a quick drying two-component epoxy adhesive.

Confocal laser reflection and fluorescence microscopy

Confocal microscopy was performed using a Leica TCS SP5 II AOBS confocal laser-scanning microscope. Immunofluorescence stainings were detected using standard confocal imaging techniques and CCs were visualized by laser reflection microscopy as previously described (5, 42). In brief, the detector and the acousto-optical beam splitter were set to allow the detection of reflected laser light. Plaque CC content was quantified from 3–4 sections per mouse using Volocity Quantitation (PerkinElmer) and depicted as ratio of total crystal reflection area to total plaque area. Investigators performing the histological analyses were blinded to the treatment of the respective animals.

Measurement of reactive oxygen species

ROS release in intact aortic segments was determined by L-012 chemiluminescence. Aortic segments of the proximal descending aorta just distal the ostium of the left subclavian artery were carefully excised and placed in chilled, modified Krebs-HEPES buffer (pH 7.4) composed of NaCl 99.01 mM, KCl 4.69 mM, $CaCl_2$ 1.87 mM, $MgSO_4$ 1.20 mM, Na-HEPES 20.0 mM, K_2HPO_4 1.03 mM, $NaHCO_3$ 25.0 mM, and D(+)glucose 11.1 mM and contained additional ascorbic acid (0.28 mM) and indomethacin (0.01 mM) {Wassmann: 2001vn}. Connective tissue was removed and aortas were cut into 2 mm segments. Chemiluminescence of aortic segments was assessed in scintillation vials containing the modified Krebs-HEPES buffer with 100 μmol/l L-012 over 15 min in a scintillation counter (Lumat LB 9501, Berthold) in 1 min intervals. The vessel segments were then dried and dry weight was determined. ROS release is calculated as relative chemiluminescence per mg aortic tissue.

Quantification of plasma cholesterol, precursors and phytosterols

Plasma concentration of cholesterol was measured by GC-flame ionization detection using 5α-cholestane as internal standard. Cholesterol precursors such as lathosterol, lanosterol, dihydro-lanosterol, and desmosterol, together with the cholesterol 5α-saturated metabolite 5α-cholestanol, and the phytosterols campesterol sitosterol, and stigmasterol were determined by GC-MS-SIM, using epicoprostanol as internal standard (43, 44). Cholesterol precursors are used as surrogate marker of cholesterol synthesis, 5α-cholestanol and plant sterols indicate sterol uptake/absorption.

Isolation of plasma lipoproteins by FPLC

For lipoprotein separation by fast performance liquid chromatography (FPLC), total plasma cholesterol levels were first determined with the Infinity Cholesterol Liquid Stable Reagent (Thermo Fisher Scientific, VA, USA). Then a 50 μl sera aliquot was pre-warmed to 37°C for 5 min followed by filtration through a PVDF 0.45 μm membrane filter. The filtered samples (20 μl) were subsequently fractionated by FPLC gel filtration on a Superose 6 PC 3.2/30 column at 4°C (GE Healthcare, Uppsala, Sweden). The elution fractions were monitored using absorbance at 280 nm, with a constant flow of 40 μl/min and fractions (40 μl) were collected beginning 18 min after sample injection. Cholesterol in each fraction was measured using the enzymatic cholesterol assay and the area under the curve for VLDL, LDL and HDL was determined in comparison to a standard of known amounts of human VLDL, LDL and HDL run in parallel.

Flow cytometry

Murine blood samples were analyzed as previously described (45). Following red blood cell lysis, the viable lymphocyte population was analyzed for sca-1-FITC (Becton Dickinson) and flk-1-PE (Becton Dickinson). Isotype identical antibodies and unstained samples served as controls in every experiment (Becton Dickinson). Cell fluorescence was measured immediately after staining using a FACS Calibur instrument (Becton Dickinson). Data were analyzed using CellQuest software (Becton Dickinson). Units of all measured components are specific events obtained after measuring 20,000 events in a pre-specified lymphocyte gate during FACS analysis. Relative lymphocyte, monocyte, and granulocyte counts were determined using a predefined gate.

Cholesterol crystal preparation

CCs were prepared from a 2 mg/ml cholesterol solution in 1-propanol. Crystallization was induced by addition of 1.5 volumes of endotoxin-free water. CCs were dried and resuspended in sterile PBS.

Cell Culture

Cells were cultured at 37°C, 5% CO_2 in a humidified atmosphere. BMDMs were derived from bone marrow isolated from tibiae and femurs of LXR$\alpha^{-/-}\beta^{-/-}$ mice (mixed genetic background on C57BL/6J and 129/Sv strains) and age and gender matched WT C57BL/6J mice. Bone marrow cells were cultured in DMEM supplemented with 10 % FCS, 10 μg/ml Ciprobay-500 and 40 ng/ml M-CSF (R&D Systems) for six days. Immortalized mouse macrophages from WT C57BL/6J mice (iMacs) were cultured in DMEM supplemented with 10% fetal calf serum (FCS) and 10 μg/ml Ciprobay-500 (Bayer).

CD binding and uptake assays

To assess CD binding to CCs, 1 mg CCs were incubated in 0.5 mM RBITC-NH2-HPβCD (rhodamine CD, Cyclolab, Hungary) for 6 h at RT. Crystals were washed 5x with PBS prior to confocal microscopic or flow cytometric analyses. For investigation of cellular CD uptake, iMacs were incubated with 20 μg CCs for 3 h. For confocal microscopic analysis living cells were imaged for 6 h after addition of 1 mM rhodamine CD mixed with unlabeled

CD in a 1:10 ratio. Uptake was saturated after 2 h. For flow cytometric analysis of CC-loaded macrophages were incubated for 3 h in 1 mM rhodamine CD and mixed with unlabeled CD in a 1:10 ratio. Following washes with PBS the cells were harvested and intracellular rhodamine fluorescence was detected using a MACSQuant analyzer (Miltenyi Biotec). Data were analyzed using FlowJo.

Cell viability assay

Cell viability was determined by incubating cells in CellTitre-Blue® reagent (Promega) at 37 °C for up to 2 h before fluorescence was measured according to the manufacture's instructions. Untreated cells served as positive control and 70 % ethanol treated cells were used as negative control (dead cells).

Radioactive cholesterol crystal dissolution assay

Radioactively labeled CCs were prepared from a 2 mg/ml cholesterol solution composed of 0.1 mCi [1,2-^{3}H]-cholesterol (Perkin Elmer) in a 1:50 (w/w) ratio with unlabeled cholesterol (Sigma) as described above. Following crystallization, the crystal solution was filtered through a 0.22 μm spin filter column to remove free [1,2-^{3}H]-cholesterol. CCs were recovered from the filter membrane and incubated overnight, shaking at 37°C in CD solutions of indicated concentrations. Filtration through 0.22 μm filter plates was used to determine the amount of solubilized [1,2-^{3}H]-cholesterol in the filtrate. The retentate was washed and subsequently incubated in ethanol for 2 h to quantify the amount of total crystalline [1,2-^{3}H]-cholesterol.

Polarization microscopy of intracellular cholesterol crystal dissolution

iMacs were incubated with 20 μg CCs for 4 h, washed with PBS and then incubated with 10 mM CD or medium control for another 3 h. Polarization images of the cells were acquired every 60 min. Crystal area was assessed by automated image analysis using Zeiss AxioVision software. Data are presented as percent of the crystal area after 4 h CC loading (time of wash step).

Lipid droplet staining

iMacs were incubated with 20 μg CCs for 3 h, washed with PBS and fixed with 4% paraformaldehyde for 30 min at RT. For LD540 staining cells were stained with 1 μg/ml fluorochrome-conjugated cholera toxin subunit B (Invitrogen) for 10 min and LD540 (46) diluted to 0.1 μg/ml in PBS for 30 min at RT. For Oil Red O staining the slides were quickly rinsed with 60% isopropanol and stained with 0.4% Oil Red O working solution (60% isopropanol) for 30 min at RT. A counterstain with Hematoxylin was performed according to standard protocols.

Analysis of crystal-derived cholesterol in macrophages

Isotope-labeled CCs were prepared from [26.26.26.27.27.27-$^{2}H_6$]-Cholesterol (D_6-cholesterol, CDN isotopes, Quebec, Canada) as described above. iMacs were incubated for 3 h with 200 μg D_6-CCs/ 1×10^{6} cells. Extracellular D_6-CCs were washed away and a control sample was harvested to assess the D6-cholesterol distribution prior to further treatment. The

remaining cells were treated for 24 h (cholesterol efflux analysis) or 48 h (cholesterol ester and oxysterol measurements) with 10 mM CD. Supernatant and cell fractions were harvested, free sterols and oxysterols were extracted and analyzed by gas chromatographic-mass spectrometric-selected ion monitoring (GC-MS-SIM).

Gas chromatographic-mass spectrometric-selected ion monitoring

Degree of esterification of D_6-cholesterol after uptake of D_6-CC into macrophages was calculated from the difference of the levels with (total D_6-cholesterol) and without (free D_6-cholesterol only) alkaline hydrolysis in cells and supernatants. After extraction of D_6-cholesterol and derivatization to its trimethyl (TMSi) silylether, gas chromatographic-mass spectrometric-selected ion monitoring (GC-MS-SIM) was performed using epicoprostanol as internal standard on m/z 464 [M^+] for the TMSi ether of D_6-cholesterol and m/z 370 [M^+] for epicoprostanol (47). The oxidized metabolite [26.26.26.27.27-$^2H_5$](25R)-26-Hydroxycholesterol (D_5-27-hydroxycholesterol) was determined from the same fractions by GC-MS-SIM on m/z 461 [M^+-90]. Authentic cholesterol and its oxidation product 27-hydroxycholesterol was measured by GC-MS-SIM on m/z 458 [M^+] and m/z 456 [M^+-90], respectively (48).

In vivo model of CC-derived reverse cholesterol transport

16-week old C57BL/6J mice were intraperitoneally injected with 15×10^6 BMDMs of either WT or LXR$\alpha^{-/-}\beta^{-/-}$ mice that were incubated for 3 h with 100 μg D_6-CCs/1×10^6 cells prior to injection. Mice were then subcutaneously injected with 2 g CD/ kg body weight or 200 μl 0.9 % NaCl as vehicle control. Feces and urine were collected every 3 h for 30 h and the pooled samples analyzed for crystal-derived D_6-cholesterol using gas chromatographic-mass spectrometric-selected ion monitoring (GC-MS-SIM). For the depiction of fecal D_6-cholesterol the radio area of D_6-cholesterol to 5α-cholestane was used. The results are presented as area under the curve of the amount of excreted D_6-cholesterol per time post CD injection.

Quantitative reverse-transcriptase PCR

For cellular gene expression analysis macrophages were incubated for 3 h with 100 μg CCs/1×10^6 cells and treated for 4 h with 10 mM CD proceeding cell disruption using a 10 G needle. For assessment of vascular gene expression, mouse aortas were excised, quickly frozen in liquid nitrogen, and homogenized with a motorized homogenizer in Trizol. RNA was isolated with peqGOLD RNA-Pure (peqLAB Biotechnology) according to the manufacturer's protocol, followed by a purification step with the RNeasy MiniElute cleanup kit (Qiagen). Total RNA was quantified by UV spectroscopy at 260 nm. The quality of the isolated RNA samples was determined by measuring the A260/A280 ratio, and the integrity of the ribosomal 28S and 18S bands was determined by agarose-gel electrophoresis. Then, 1 μg of the isolated total RNA was reverse transcribed using the Omniscript RT Kit (Qiagen) according to the manufactures protocol. The single-stranded cDNA was amplified by real-time quantitative reverse transcription-polymerase chain reaction with the TaqMan system using commercially available Taqman® probes (*Abca1* Mm00442646_m1, *Abcg1* Mm00437390_m1, Applied Biosystems). *Abca*1 and *Abcg*1 mRNA expression was normalized to 18S (Mm03928990_g1, Taqman® probes, Applied Biosystems).

Western blotting

Macrophages were incubated for 3 h with 100 μg CCs/ 1×10^6 cells and treated for 24 h with 10 mM CD. LXR agonist T0901317 (Sigma) was used as a positive control for LXR activation. Cells were lysed on ice for 30 min with 1x RIPA buffer (20 mM Tris-HCl pH 7.4, 150 mM NaCl, 1 mM EDTA, 1% Triton X-100, 10% glycerol, 0.1% SDS, 0.5% deoxycholate, 0.1 μM PMSF) supplemented with complete protease inhibitors (Roche Biochemicals). Protein concentrations were determined by BCA assay (Pierce) and equal amounts of protein were loaded on 4–12% pre-cast SDS-PAGE gels (Novex, Invitrogen) with MOPS running buffer (Novex, Invitrogen). Proteins were transferred to a PVDF membrane (Millipore) and membranes were blocked in 3% BSA in TBS with Tween-20, incubated with mouse monoclonal ABCA1 antibody (MAB10005, Millipore) and rabbit monoclonal β-actin antibody (Li-Cor Biosciences) overnight at 4°C. The membranes were washed and incubated with secondary anti-mouse and anti-rabbit antibodies (Li-Cor Biosciences) for 45 min in the dark. Immunoreactivity was visualized by near-infrared detection (Odyssey, LICOR).

Gene expression profiling by Illumina Bead Chip technology

Biotin labeled cRNA was generated using the TargetAmp Nano-g Biotin-aRNA Labeling Kit for the Illumina System (Epicentre). Biotin labeled cRNA (750 ng) was hybridized to Human HT-12V3 Beadchips (Illumina) and scanned on an Illumina iScan or HiScanSQ system.

Primary data and quality control analysis of microarray data

Raw intensity data were processed and exported with Genome Studio V2011.1 (Copyright© 2003–2011 Illumina). All array data were imported into Partek® Genomics SuiteTM version 6.6 (PGS, Copyright© 2012 Partek Incorporated). Quality control assessments including principle component analysis and box-whisker plots to visualize expression distribution were applied.

Bioinformatic analysis of microarray data

Non-normalized data (log2) were quantile normalized and transcripts with variable expression within the dataset as well as differentially expressed (DE) genes between the different conditions were calculated using two-way ANOVA models including batch correction sentrix bar code and gender where applicable. For analyses of the microarray data on BMDMs derived from WT or LXR$\alpha^{-/-}\beta^{-/-}$ mice (GSE67013), DE genes were defined by a fold change (FC) greater 2 and p-value<0.05. Gene Set Enrichment Analysis (GSEA) was used to determine whether a defined set of genes is statistically significant between two different states. A set of genes is statistically significant enriched when the p-value is ≤ 0.05 and the false discovery rate (FDR) is ≤ 0.25 comparing two different states. GSEA was performed with 1000 permutations against a list of LXR target genes generated from the LXR target genes identified by Heinz *et al.* (30) (Table S1). For analyses of the microarray data on descending aortas of mice from the bone-marrow transplantation model (GSE67011), DE genes were defined by a FC greater 1.3 and p-value<0.05. To link the DE genes for CD vs. Control to prior knowledge we performed Gene Ontology Enrichment

Analysis (GOEA) using the Cytoscape (http://www.cytoscape.org/) plug-in BiNGO (v2.44) (49). The FDR threshold was set to 0.05 to include only significant results. The Cytoscape plugins Enrichment Map (v1.1) (50) and Word Cloud (51) were used to visualize GO networks. The cutoff for the Jaccard coefficient was set to 0.51 and the FDR q-value to 0.1. Gene expression of genes relevant for the NLRP3 inflammasome pathway was visualized in Partek Pathway.

Cholesterol quantification in urine of NPC1 patients

NPC1-deficient patients receive weekly infusions of 2000 mg CD/kg bodyweight over 8 h (ClinicalTrial.gov NCT01747135). Urine samples from three individual NPC1 patients were collected at indicated timepoints upon start of the intravenous CD application. Urine cholesterol concentration was determined by GC-MS-SIM as described above and normalized to urine creatinine excretion. The study protocol followed procedures in accordance with the Helsinki Declaration of 1975 (revised 1983) and the I-IND (Individual-Investigative New Drug) protocol was approved by the FDA. Written informed consent was obtained from the legal guardians of all subjects.

Patient cohort for human atherosclerotic carotid plaques

Patients with high-grade internal carotid stenosis (≥70%) or ischemic stroke within the last month were recruited at Department of Neurology, Oslo University Hospital Rikshospitalet. The carotid stenosis was diagnosed and classified by precerebral color duplex and CT angiography according to consensus criteria. As for ultrasound examination, the total extracranial part of the carotid artery was examined with B-mode and Doppler analyses. Ultrasound plaque appearance in terms of echogenicity was classified according to consensus criteria (52). Exclusion criteria were heart failure, liver disease, kidney disease, and severe concomitant disease such as infection, connective tissue disease, or malignancy. The Regional Health Authorities of South-Eastern and Western Norway approved the study protocols (REK no: S-0923a 2009/6065). The study confirms with the principles outlined in the Declaration of Helsinki for use of human tissue or subjects. Signed informed consent was obtained from all participants.

Culturing of human atherosclerotic carotid plaques

Biopsies from atherosclerotic carotid plaques (n=10), obtained from patients that had been suffering from symptoms within 1 month and or stenosis degree of ≥ 70%, were placed in Dulbecco’s modified Eagle’s medium ([D-MEM]/F12; Gibco) enriched with 30 mg/ml endotoxin free and fatty acid free bovine serum albumin (Sigma). The biopsies containing atherosclerotic plaques of each patient were split into two macroscopically equal pieces and incubated for 16 h with 10 mM CD or PBS. The plaque biopsies were then split into two pieces and either placed in RNA Later (Qiagen) for RNA analysis or snap frozen for lipid analysis. Plaque supernatants were collected, centrifuged (1700 *g* for 5 min, 4°C) and snap frozen before being stored at −80°C prior to further analysis.

Sterol and Oxyphytosterol analyses from dried plaque tissue and supernatant

Excised and worked-up as described before plaque tissue was dried in a SavantTM SpeedVacTM concentrator (Thermo Fisher Scientific, Schwerte, Germany) for 24 h. Cholesterol, non-cholesterol sterols and oxysterols were extracted from dry weight aliquots using Folch reagent (chloroform/methanol; 2:1; (v:v); with 0.25 mg BHT added per mL solvent) per 10 mg dried plaque tissue tissue. Extraction was performed for 24 h at 4°C in a dark cold room. The extracts were kept at −20°C until analysis. One ml of supernatant and one ml of the Folch extract of plaque tissue underwent alkaline hydrolysis, extraction of the free sterols and oxysterols, silylation to their corresponding (di)trimethylsilyl ethers prior to gas chromatographic separation and detection either by flame ionization detection (for cholesterol using 5α-cholestane as internal standard) or by mass selective detection (for non-cholesterol sterols or oxysterols using epicoprostanol and the corresponding deuterium labeled oxysterols as internal standards, respectively) as described in detail previously (44, 53).

Nanostring analysis of human atherosclerotic carotid plaques

Plaque pieces were cut in similar sizes and homogenization was performed with a FastPrep® 24 instrument (≈6 m/s, MD Biomedicals) three times 40 seconds with zirconium oxide beads (Bertin Tech) (six 2.8 mm beads and 0.8 g 1.4 mm beads per sample) in Isol-RNA Lysis Reagent (VWR, 5Prime). The aqueous phase was isolated after adding chloroform and centrifugation (13000 rpm, 15 min, 4°C) and RNA was isolated further with RNeasy microkit (Qiagen,). Nanodrop spectrophotometer (ND-1000, Saveen Werner) was used to measure RNA concentration and 100 ng was applied from each sample for RNA expression analysis, running one strip of 12 samples at a time at nCounter ® analysis system (Nanostring Technologies). The procedure was performed according to the manufacturer's instructions. Kit used was a fixed codeset for mRNA analysis, nCounter GX Human Immunology Kit v2 (Nanostring Technologies), spiked with another 30 probes of our own choice (nCounter Panel Plus, Table S2).

Bioinformatic analysis of Nanostring data

Number of mRNA molecules counted was imported into NSolver with default settings, corrected and normalized against non-detected background (mean of negative controls + 2 standard deviations), instrumental variations (positive controls) and against the reference genes annotated in the kit that were found to be stable (RPL19, EEF1G, TUBB, OAZ1, GAPDH, POLRA2, G6PD, HPRT1) (NSolver Analysis Software 2.5.34 Nanostring Technologies). The data was further imported into Partek Genomics Suite 6.6, non-detected values were set to 1 and the data was batch-corrected for the interaction strip and patient. GSEA was performed with 1000 permutations on the dataset using a LXR target gene list generated from the direct LXR target genes identified in Pehkonen *et al.* (54) (Table S3). The result is considered statistically significant enriched when the p-value is ≤ 0.05 and the false discovery rate (FDR) is ≤ 0.25 comparing two different states. DE genes calculated by three-way ANOVA were defined by a FC greater than 1.3 and p-value<0.05. To link the DE genes for CD vs. PBS to prior knowledge we performed GOEA using the Cytoscape (http://www.cytoscape.org/) plug-in BiNGO (v2.44) (49). The FDR threshold was set to 0.05 to

include only significant results. The Cytoscape plugins Enrichment Map (v1.1) (50) and Word Cloud (51) were used to visualize GO networks. The cutoff for the Jaccard coefficient was set to 0.51 and the FDR q-value to 0.1. Gene expression of genes relevant for the NLRP3 inflammasome pathway was visualized in Partek Pathway (55, 56).

Statistics

Unless otherwise indicated data are presented as mean ± standard error of mean (s.e.m.). For statistical analysis, two-tailed, unpaired Student's t-test and ANOVA for multiple comparisons were employed. Post-hoc comparisons were performed with the Tukey test. $p<0.05$ was considered statistically significant. All significant p-values are included in Table S4. Basic analyses were performed with Excel (Microsoft) and Prism (GraphPad Software, Inc.). Furthermore, Volocity Quantitation (PerkinElmer) was used for image analysis and gene expression data was analyzed with Partek Genomics Suite (Partek) using ANOVA models and GSEA results were plotted using Sigmaplot 12.2.

Supplementary Material

Refer to Web version on PubMed Central for supplementary material.

Acknowledgments

We appreciate the great technical assistance of Catharina Lahrmann, Anna Glubokovskih, Gudrun Hack und Silke Bellinghausen (University of Bonn, Bonn, Germany), Anne Marstad (Norwegian University of Science and Technology, Trondheim, Norway) and Kirsten Krohg Sørensen (Oslo University Hospital, Oslo, Norway). We thank Caroline Hastings (Children's Hospital & Research Center Oakland, Oakland, CA, USA) for help with the acquisition of samples from NPC patients and greatly appreciate the contribution of the Hadley Hope Fund (Medford, OR, USA). 2-hydroxypropyl-β-cyclodextrin as well as 2-hydroxypropyl-β-cyclodextrin-rhodamine was kindly provided by CTD Holdings, Inc., Alachua, FL, USA. LD540 was generously provided by Christoph Thiele (University of Bonn, Bonn, Germany).

Funding: This work was funded by grants of the National Institutes of Health R01-HL093262, R21-HL113907-01 (to E.L.), HL112661-01 (to M.L.F. and E.L.), HL101274 (to M.L.F.), HL107653 (to A.R.T.), by the Research Council of Norway through its Centres of Excellence funding scheme, project number 223255/F50 (to S.S.B, E.L. and T.E.), by BONFOR (to S.Z. and N.B.), by the Robert A. Welch Foundation (E-0004, to J.A.G), by the Swedish Science Council (H2416223, to J.A.G.) and by grants of the Deutsche Forschungsgemeinschaft (DFG) (to E.L., J.L.S. and J.T.). E.L, M.T.H. and J.L.S. are members of the Excellence cluster ImmunoSensation funded by the DFG.

References

1. Robinson JG, Farnier M, Krempf M, Bergeron J, Luc G, Averna M, Stroes ES, Langslet G, Raal FJ, Shahawy ME, Koren MJ, Lepor NE, Lorenzato C, Pordy R, Chaudhari U, Kastelein JJP. ODYSSEY LONG TERM Investigators, Efficacy and Safety of Alirocumab in Reducing Lipids and Cardiovascular Events. N Engl J Med. 2015; doi: 10.1056/NEJMoa1501031
2. Sabatine MS, Giugliano RP, Wiviott SD, Raal FJ, Blom DJ, Robinson J, Ballantyne CM, Somaratne R, Legg J, Wasserman SM, Scott R, Koren MJ, Stein EA. Open-Label Study of Long-Term Evaluation against LDL Cholesterol (OSLER) Investigators, Efficacy and Safety of Evolocumab in Reducing Lipids and Cardiovascular Events. N Engl J Med. 2015 150315080057008.
3. Montalescot G, Sechtem U, Achenbach S, Andreotti F, Arden C, Budaj A, Bugiardini R, Crea F, Cuisset T, Di Mario C, Ferreira JR, Gersh BJ, Gitt K, Hulot JS, Marx N, Opie LH, Pfisterer M, Prescott E, Ruschitzka F, Sabate M, Senior R, Taggart DP, van der Wall EE, Vrints CJM, Zamorano JL, Baumgartner H, Bax JJ, Bueno H, Dean V, Deaton C, Erol C, Fagard R, Ferrari R, Hasdai D, Hoes AW, Kirchhof P, Knuuti J, Kolh P, Lancellotti P, Linhart A, Nihoyannopoulos P, Piepoli MF, Ponikowski P, Sirnes PA, Tamargo JL, Tendera M, Torbicki A, Wijns W, Windecker S, Valgimigli

M, Bueno H, Claeys MJ, Donner-Banzhoff N, Erol C, Frank H, Funck-Brentano C, Gaemperli O, Gonzalez-Juanatey JR, Hamilos M, Husted S, James SK, Kervinen K, Kristensen SD, Maggioni AP, Piepoli MF, Pries AR, Romeo F, Ryden L, Simoons ML, Steg PG, Timmis A, Yildirir A. Task Force Members, ESC Committee for Practice Guidelines (CPG). 2013 ESC guidelines on the management of stable coronary artery disease: The Task Force on the management of stable coronary artery disease of the European Society of Cardiology. Eur Heart J. 2013; 34:2949–3003. Document Reviewers. [PubMed: 23996286]

4. Sheedy FJ, Grebe A, Rayner KJ, Kalantari P, Ramkhelawon B, Carpenter SB, Becker CE, Ediriweera HN, Mullick AE, Golenbock DT, Stuart LM, Latz E, Fitzgerald KA, Moore KJ. CD36 coordinates NLRP3 inflammasome activation by facilitating intracellular nucleation of soluble ligands into particulate ligands in sterile inflammation. Nat Immunol. 2013; 14:812–820. [PubMed: 23812099]
5. Duewell P, Kono H, Rayner KJ, Sirois CM, Vladimer G, Bauernfeind FG, Abela GS, Franchi L, Nuñez G, Schnurr M, Espevik T, Lien E, Fitzgerald KA, Rock KL, Moore KJ, Wright SD, Hornung V, Latz E. NLRP3 inflammasomes are required for atherogenesis and activated by cholesterol crystals. Nature. 2010; 464:1357–1361. [PubMed: 20428172]
6. Ridker PM, Thuren T, Zalewski A, Libby P. Interleukin-1β inhibition and the prevention of recurrent cardiovascular events: rationale and design of the Canakinumab Anti-inflammatory Thrombosis Outcomes Study (CANTOS). Am Heart J. 2011; 162:597–605. [PubMed: 21982649]
7. Warnatsch A, Ioannou M, Wang Q, Papayannopoulos V. Inflammation. Neutrophil extracellular traps license macrophages for cytokine production in atherosclerosis. Science. 2015; 349:316–320. [PubMed: 26185250]
8. Nymo S, Niyonzima N, Espevik T, Mollnes TE. Cholesterol crystal-induced endothelial cell activation is complement-dependent and mediated by TNF. Immunobiology. 2014; 219:786–792. [PubMed: 25053140]
9. Samstad EO, Niyonzima N, Nymo S, Aune MH, Ryan L, Bakke SS, Lappegård KT, Brekke OL, Lambris JD, Damås JK, Latz E, Mollnes TE, Espevik T. Cholesterol crystals induce complement-dependent inflammasome activation and cytokine release. J Immunol. 2014; 192:2837–2845. [PubMed: 24554772]
10. Kiyotake R, Oh-Hora M, Ishikawa E, Miyamoto T, Ishibashi T, Yamasaki S. Human Mincle Binds to Cholesterol Crystals and Triggers Innate Immune Responses. J Biol Chem. 2015 jbc.M115.645234.
11. Rayner KJ, Esau CC, Hussain FN, McDaniel AL, Marshall SM, van Gils JM, Ray TD, Sheedy FJ, Goedeke L, Liu X, Khatsenko OG, Kaimal V, Lees CJ, Fernández-Hernando C, Fisher EA, Temel RE, Moore KJ. Inhibition of miR-33a/b in non-human primates raises plasma HDL and lowers VLDL triglycerides. Nature. 2011; 478:404–407. [PubMed: 22012398]
12. Gould S, Scott RC. 2-Hydroxypropyl-β-cyclodextrin (HP-β-CD): A toxicology review. Food and Chemical Toxicology. 2005; 43:1451–1459. [PubMed: 16018907]
13. Loftsson T, Jarho P, Másson M, Järvinen T. Cyclodextrins in drug delivery. Expert Opin Drug Deliv. 2005; 2:335–351. [PubMed: 16296758]
14. Liu SM. Cyclodextrins differentially mobilize free and esterified cholesterol from primary human foam cell macrophages. J Lipid Res. 2003; 44:1156–1166. [PubMed: 12671029]
15. Kritharides L, Kus M, Brown AJ, Jessup W, Dean RT. Hydroxypropyl-beta-cyclodextrin-mediated efflux of 7-ketocholesterol from macrophage foam cells. J Biol Chem. 1996; 271:27450–27455. [PubMed: 8910326]
16. Atger VM, de la Llera Moya M, Stoudt GW, Rodrigueza WV, Phillips MC, Rothblat GH. Cyclodextrins as catalysts for the removal of cholesterol from macrophage foam cells. J Clin Invest. 1997; 99:773–780. [PubMed: 9045882]
17. Mackay DS, Jones PJH. Plasma noncholesterol sterols: current uses, potential and need for standardization. Curr Opin Lipidol. 2012; 23:241–247. [PubMed: 22510807]
18. Getz GS, Reardon CA. Animal models of atherosclerosis. Arterioscler Thromb Vasc Biol. 2012; 32:1104–1115. [PubMed: 22383700]
19. Hewing B, Fisher EA. Preclinical mouse models and methods for the discovery of the causes and treatments of atherosclerosis. Expert Opin Drug Discov. 2012; 7:207–216. [PubMed: 22468952]

20. Rayner KJ, Sheedy FJ, Esau CC, Hussain FN, Temel RE, Parathath S, van Gils JM, Rayner AJ, Chang AN, Suárez Y, Fernández-Hernando C, Fisher EA, Moore KJ. Antagonism of miR-33 in mice promotes reverse cholesterol transport and regression of atherosclerosis. J Clin Invest. 2011; 121:2921–2931. [PubMed: 21646721]
21. Tabas I. Consequences of cellular cholesterol accumulation: basic concepts and physiological implications. J Clin Invest. 2002; 110:905–911. [PubMed: 12370266]
22. Repa JJ, Mangelsdorf DJ. The liver X receptor gene team: potential new players in atherosclerosis. Nat Med. 2002; 8:1243–1248. [PubMed: 12411951]
23. Tall AR, Yvan-Charvet L. Cholesterol, inflammation and innate immunity. Nature Reviews Immunology. 2015; 15:104–116.
24. Reboldi A, Dang EV, McDonald JG, Liang G, Russell DW, Cyster JG. Inflammation. 25-Hydroxycholesterol suppresses interleukin-1-driven inflammation downstream of type I interferon. Science. 2014; 345:679–684. [PubMed: 25104388]
25. Khera AV, Cuchel M, de la Llera-Moya M, Rodrigues A, Burke MF, Jafri K, French BC, Phillips JA, Mucksavage ML, Wilensky RL, Mohler ER, Rothblat GH, Rader DJ. Cholesterol efflux capacity, high-density lipoprotein function, and atherosclerosis. N Engl J Med. 2011; 364:127–135. [PubMed: 21226578]
26. Rohatgi A, Khera A, Berry JD, Givens EG, Ayers CR, Wedin KE, Neeland IJ, Yuhanna IS, Rader DR, de Lemos JA, Shaul PW. HDL cholesterol efflux capacity and incident cardiovascular events. N Engl J Med. 2014; 371:2383–2393. [PubMed: 25404125]
27. Rader DJ, Puré E. Lipoproteins, macrophage function, and atherosclerosis: beyond the foam cell? Cell Metab. 2005; 1:223–230. [PubMed: 16054067]
28. Janowski BA, Willy PJ, Devi TR, Falck JR, Mangelsdorf DJ. An oxysterol signalling pathway mediated by the nuclear receptor LXR alpha. Nature. 1996; 383:728–731. [PubMed: 8878485]
29. Subramanian A, Tamayo P, Mootha VK, Mukherjee S, Ebert BL, Gillette MA, Paulovich A, Pomeroy SL, Golub TR, Lander ES, Mesirov JP. Gene set enrichment analysis: a knowledge-based approach for interpreting genome-wide expression profiles. Proc Natl Acad Sci USA. 2005; 102:15545–15550. [PubMed: 16199517]
30. Heinz S, Benner C, Spann N, Bertolino E, Lin YC, Laslo P, Cheng JX, Murre C, Singh H, Glass CK. Simple combinations of lineage-determining transcription factors prime cis-regulatory elements required for macrophage and B cell identities. Mol Cell. 2010; 38:576–589. [PubMed: 20513432]
31. Repa JJ, Turley SD, Lobaccaro JA, Medina J, Li L, Lustig K, Shan B, Heyman RA, Dietschy JM, Mangelsdorf DJ. Regulation of absorption and ABC1-mediated efflux of cholesterol by RXR heterodimers. Science. 2000; 289:1524–1529. [PubMed: 10968783]
32. Liu B, Li H, Repa JJ, Turley SD, Dietschy JM. Genetic variations and treatments that affect the lifespan of the NPC1 mouse. J Lipid Res. 2008; 49:663–669. [PubMed: 18077828]
33. Taylor AM, Liu B, Mari Y, Liu B, Repa JJ. Cyclodextrin mediates rapid changes in lipid balance in Npc1−/− mice without carrying cholesterol through the bloodstream. J Lipid Res. 2012; 53:2331–2342. [PubMed: 22892156]
34. Mayor A, Martinon F, De Smedt T, Pétrilli V, Tschopp J. A crucial function of SGT1 and HSP90 in inflammasome activity links mammalian and plant innate immune responses. Nat Immunol. 2007; 8:497–503. [PubMed: 17435760]
35. Castrillo A, Joseph SB, Vaidya SA, Haberland M, Fogelman AM, Cheng G, Tontonoz P. Crosstalk between LXR and toll-like receptor signaling mediates bacterial and viral antagonism of cholesterol metabolism. Mol Cell. 2003; 12:805–816. [PubMed: 14580333]
36. Feingold KR, Grunfeld C. The acute phase response inhibits reverse cholesterol transport. J Lipid Res. 2010; 51:682–684. [PubMed: 20071695]
37. De Nardo D, Labzin LI, Kono H, Seki R, Schmidt SV, Beyer M, Xu D, Zimmer S, Lahrmann C, Schildberg FA, Vogelhuber J, Kraut M, Ulas T, Kerksiek A, Krebs W, Bode N, Grebe A, Fitzgerald ML, Hernandez NJ, Williams BRG, Knolle P, Kneilling M, Röcken M, Lütjohann D, Wright SD, Schultze JL, Latz E. High-density lipoprotein mediates anti-inflammatory reprogramming of macrophages via the transcriptional regulator ATF3. Nat Immunol. 2014; 15:152–160. [PubMed: 24317040]

38. Kappus MS, Murphy AJ, Abramowicz S, Ntonga V, Welch CL, Tall AR, Westerterp M. Activation of liver X receptor decreases atherosclerosis in Ldlr$^{-/-}$mice in the absence of ATP-binding cassette transporters A1 and G1 in myeloid cells. Arterioscler Thromb Vasc Biol. 2014; 34:279–284. [PubMed: 24311381]
39. Joseph SB, McKilligin E, Pei L, Watson MA, Collins AR, Laffitte BA, Chen M, Noh G, Goodman J, Hagger GN, Tran J, Tippin TK, Wang X, Lusis AJ, Hsueh WA, Law RE, Collins JL, Willson TM, Tontonoz P. Synthetic LXR ligand inhibits the development of atherosclerosis in mice. Proc Natl Acad Sci USA. 2002; 99:7604–7609. [PubMed: 12032330]
40. Feig JE, Pineda-Torra I, Sanson M, Bradley MN, Vengrenyuk Y, Bogunovic D, Gautier EL, Rubinstein D, Hong C, Liu J, Wu C, van Rooijen N, Bhardwaj N, Garabedian M, Tontonoz P, Fisher EA. LXR promotes the maximal egress of monocyte-derived cells from mouse aortic plaques during atherosclerosis regression. J Clin Invest. 2010; 120:4415–4424. [PubMed: 21041949]
41. Li X, Yeh V, Molteni V. Liver X receptor modulators: a review of recently patented compounds (2007 – 2009). Expert Opin Ther Pat. 2010; 20:535–562. [PubMed: 20302451]
42. Hornung V, Bauernfeind F, Halle A, Samstad EO, Kono H, Rock KL, Fitzgerald KA, Latz E. Silica crystals and aluminum salts activate the NALP3 inflammasome through phagosomal destabilization. Nat Immunol. 2008; 9:847–856. [PubMed: 18604214]
43. Lütjohann D, Hahn C, Prange W, Sudhop T, Axelson M, Sauerbruch T, von Bergmann K, Reichel C. Influence of rifampin on serum markers of cholesterol and bile acid synthesis in men. Int J Clin Pharmacol Ther. 2004; 42:307–313. [PubMed: 15222722]
44. Lütjohann D, Brzezinka A, Barth E, Abramowski D, Staufenbiel M, von Bergmann K, Beyreuther K, Multhaup G, Bayer TA. Profile of cholesterol-related sterols in aged amyloid precursor protein transgenic mouse brain. J Lipid Res. 2002; 43:1078–1085. [PubMed: 12091492]
45. Zimmer S, Steinmetz M, Asdonk T, Motz I, Coch C, Hartmann E, Barchet W, Wassmann S, Hartmann G, Nickenig G. Activation of endothelial toll-like receptor 3 impairs endothelial function. Circ Res. 2011; 108:1358–1366. [PubMed: 21493895]
46. Spandl J, White DJ, Peychl J, Thiele C. Live Cell Multicolor Imaging of Lipid Droplets with a New Dye, LD540. Traffic. 2009; 10:1579–1584. [PubMed: 19765264]
47. Lütjohann D, Stroick M, Bertsch T, Kühl S, Lindenthal B, Thelen K, Andersson U, Björkhem I, Bergmann KV, Fassbender K. High doses of simvastatin, pravastatin, and cholesterol reduce brain cholesterol synthesis in guinea pigs. Steroids. 2004; 69:431–438. [PubMed: 15219793]
48. Lütjohann D, Breuer O, Ahlborg G, Nennesmo I, Sidén A, Diczfalusy U, Björkhem I. Cholesterol homeostasis in human brain: evidence for an age-dependent flux of 24S-hydroxycholesterol from the brain into the circulation. Proc Natl Acad Sci USA. 1996; 93:9799–9804. [PubMed: 8790411]
49. Maere S, Heymans K, Kuiper M. BiNGO: a Cytoscape plugin to assess overrepresentation of gene ontology categories in biological networks. Bioinformatics. 2005; 21:3448–3449. [PubMed: 15972284]
50. Merico D, Isserlin R, Stueker O, Emili A, Bader GD, Ravasi T. Enrichment map: a network-based method for gene-set enrichment visualization and interpretation. PLoS ONE. 2010; 5:e13984. [PubMed: 21085593]
51. Oesper L, Merico D, Isserlin R, Bader GD. WordCloud: a Cytoscape plugin to create a visual semantic summary of networks. Source Code Biol Med. 2011; 6:7. [PubMed: 21473782]
52. Brott TG, Halperin JL, Abbara S, Bacharach JM, Barr JD, Bush RL, Cates CU, Creager MA, Fowler SB, Friday G, Hertzberg VS, McIff EB, Moore WS, Panagos PD, Riles TS, Rosenwasser RH, Taylor AJ. American College of Cardiology, American Stroke Association, American Association of Neurological Surgeons, American College of Radiology, American American College of Radiology, Society of NeuroInterventional Surgery, Society for Vascular Medicine, Society for Vascular Surgery. 2011 ASA/ACCF/AHA/AANN/AANS/ACR/ASNR/CNS/SAIP/SCAI/SIR/SNIS/SVM/SVS guideline on the management of patients with extracranial carotid and vertebral artery disease. A report of the American College of Cardiology Foundation/American Heart Association Task Force on Practice Guidelines, and the American Stroke Association, American Association of Neuroscience Nurses, American Association of Neurological Surgeons, American College of Radiology, American Society of Neuroradiology, Congress of Neurological Surgeons, Society of Atherosclerosis Imaging and Prevention, Society for Cardiovascular

Angiography and Interventions, Society of Interventional Radiology, Society of NeuroInterventional Surgery, Society for Vascular Medicine, and Society for Vascular Surgery. Circulation. 2011; 124:e54–130. [PubMed: 21282504]

53. Mackay DS, Jones PJH, Myrie SB, Plat J, Lütjohann D. Methodological considerations for the harmonization of non-cholesterol sterol bio-analysis. J Chromatogr B Analyt Technol Biomed Life Sci. 2014; 957:116–122.
54. Pehkonen P, Welter-Stahl L, Diwo J, Ryynänen J, Wienecke-Baldacchino A, Heikkinen S, Treuter E, Steffensen KR, Carlberg C. Genome-wide landscape of liver X receptor chromatin binding and gene regulation in human macrophages. BMC Genomics. 2012; 13:50. [PubMed: 22292898]
55. Mathiesen EB, Bønaa KH, Joakimsen O. Echolucent plaques are associated with high risk of ischemic cerebrovascular events in carotid stenosis: the tromsø study. Circulation. 2001; 103:2171–2175. [PubMed: 11331258]
56. Olofsson PS, Jatta K, Wågsäter D, Gredmark S, Hedin U, Paulsson-Berne G, Söderberg-Nauclér C, Hansson GK, Sirsjö A. The antiviral cytomegalovirus inducible gene 5/viperin is expressed in atherosclerosis and regulated by proinflammatory agents. Arterioscler Thromb Vasc Biol. 2005; 25:e113–6. [PubMed: 15890971]

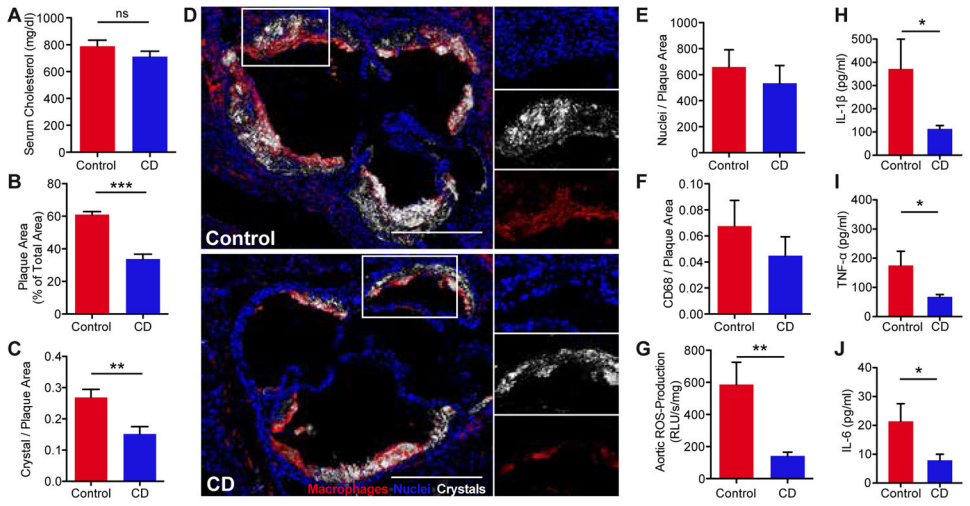

Fig. 1. CD treatment impairs murine atherogenesis

ApoE$^{-/-}$ mice were fed a cholesterol-rich diet for eight weeks and concomitantly treated with 2 g CD/ kg body weight or vehicle control by subcutaneous injection twice a week (n=7–8 per group). **(A)** Plasma cholesterol levels. **(B)** Atherosclerotic plaque area relative to total arterial wall area. **(C)** Plaque CC load shown as ratio of crystal reflection area to plaque area. **(D)** Representative images of the aortic plaques obtained by confocal laser reflection microscopy. Macrophages stained with anti-CD68 antibodies (red), reflection signal of CCs (white), nuclei stained with Hoechst (blue). Enlarged area (white boxes). Scale bars indicate 500 μm. **(E)** Plaque cellularity shown as ratio of nuclei to plaque area. **(F)** Plaque macrophage load shown as ratio of CD68 fluorescence area to total plaque area. **(G)** Aortic superoxide production determined by L-012 chemiluminescence. Plasma **(H)** IL-1β, **(I)** TNF-α and **(J)** IL-6 levels. Data are shown as mean + s.e.m., Control vs. CD, unpaired two-tailed Student's t test; ***p < 0.001, **p < 0.01, *p < 0.05, ns = not significant.

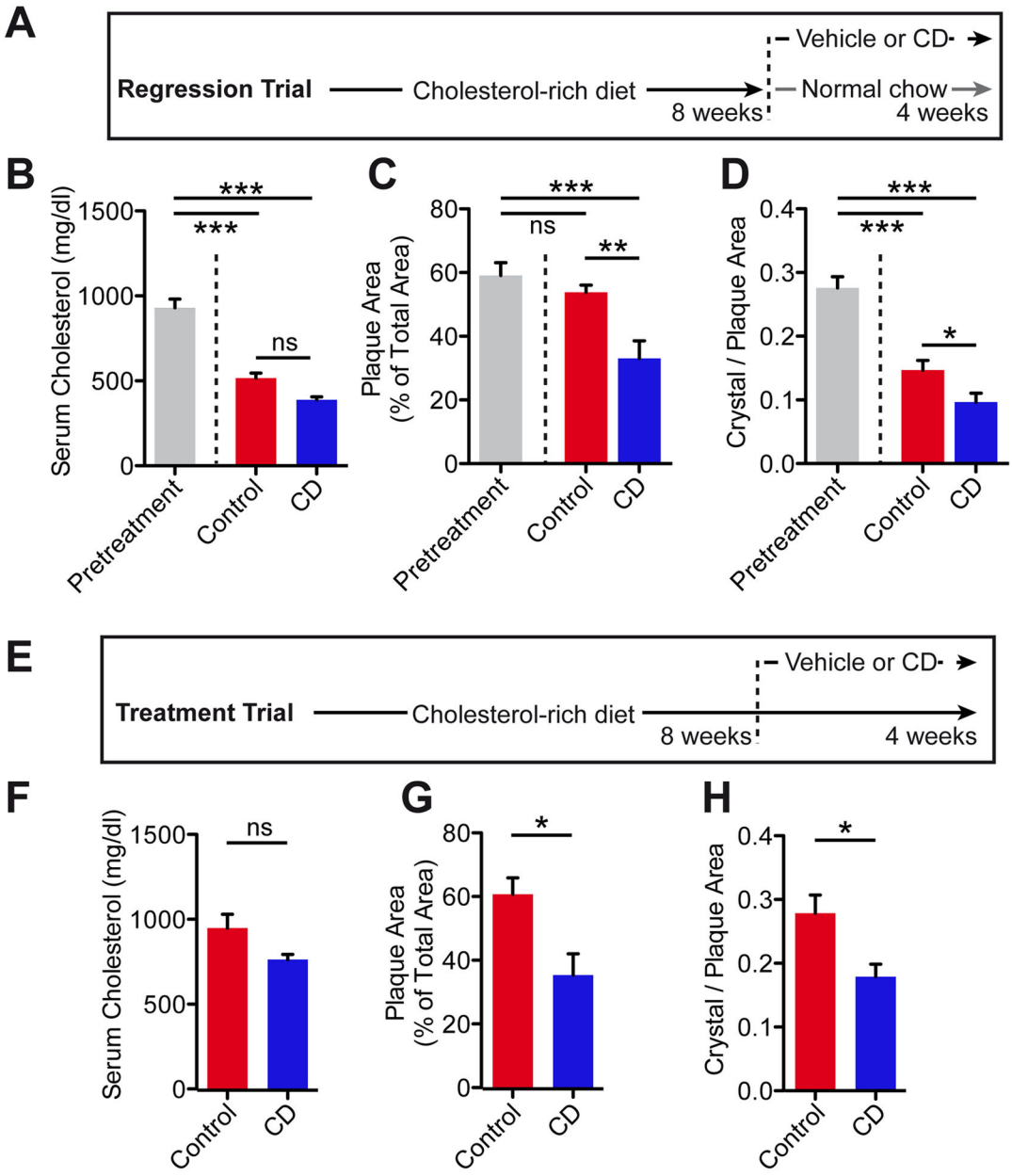

Fig. 2. CD treatment facilitates regression of murine atherosclerosis

ApoE$^{-/-}$ mice were fed a cholesterol-rich diet for eight weeks to induce advanced atherosclerotic lesions. Then the diet was either changed to a normal chow **(A–D)** or the cholesterol-rich diet was continued **(E–H)** for another four weeks. Mice were simultaneously treated with 2 g CD/ kg body weight or vehicle control twice a week (n=6–8 per group). **(B, F)** Plasma cholesterol levels. **(C, G)** Atherosclerotic plaque area relative to total arterial wall area. **(D, H)** Plaque CC load shown as ratio of crystal reflection area to plaque area. Data are shown as mean + s.e.m., Control vs. CD, unpaired two-tailed Student's t test; ***p < 0.001, **p < 0.01, *p < 0.05, ns = not significant.

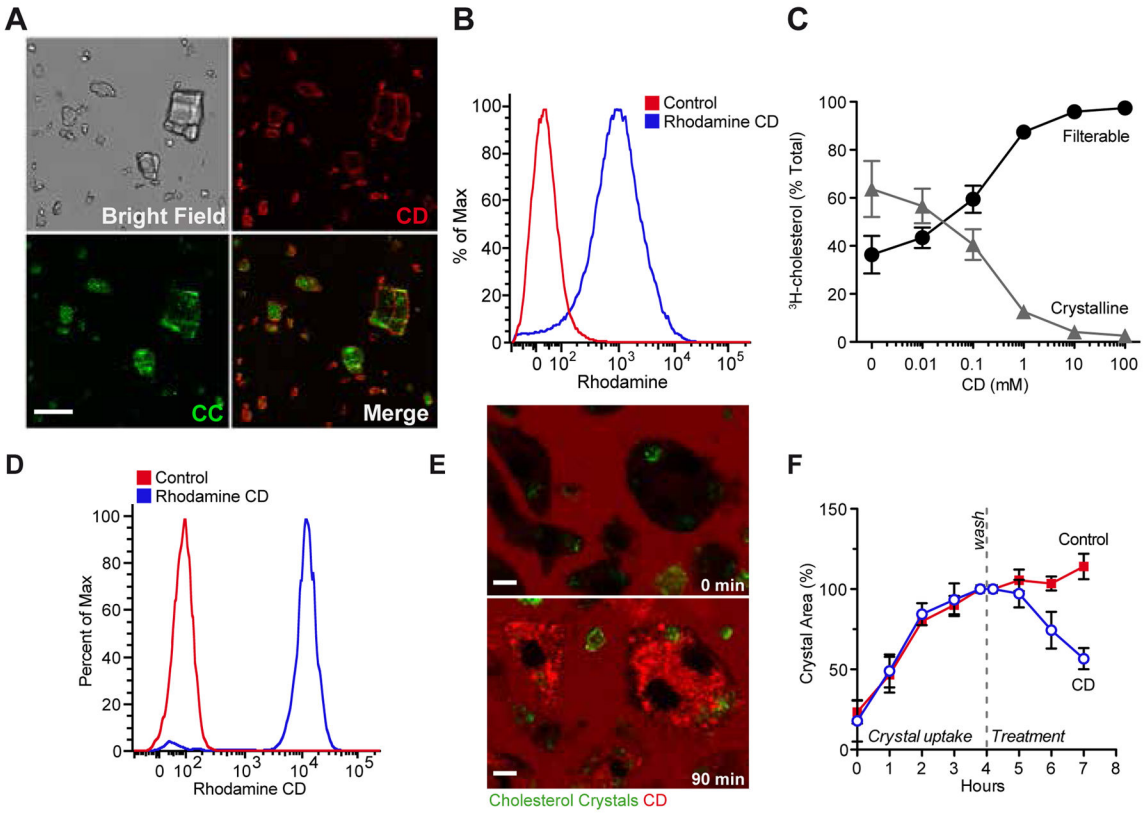

Fig. 3. CD interacts with and dissolves extra- and intracellular CCs

(A, B) 1 mg CCs were incubated in 0.5 mM rhodamine labeled CD or PBS as control. **(A)** Representative images obtained by confocal laser reflection microscopy. Scale bar equals 20 μm. **(B)** Quantification of rhodamine fluorescence on CCs by flow cytometry. **(C)** ^{3}H-CC were incubated in CD solutions of indicated concentrations overnight shaking at 37°C. Upon filtration through 0.22 μm filter plates radioactivity was determined in the filtrate (filterable/solubilized) and the retentate (crystalline). **(D, E)** iMacs loaded with 200 μg CC/1×10^{6} cells for 3 h prior to incubation with 1 mM rhodamine labeled CD. **(D)** Quantification of rhodamine fluorescence by flow cytometry. **(E)** Representative images obtained by confocal microscopy; rhodamine labeled CD (red), laser reflection signal (green). Scale bars equal 5 μm. **(F)** Intracellular CC dissolution in BMDMs treated with 10 mM CD or control for indicated times determined by polarization microscopy. Data are shown as mean +/− s.e.m of at least three independent experiments.

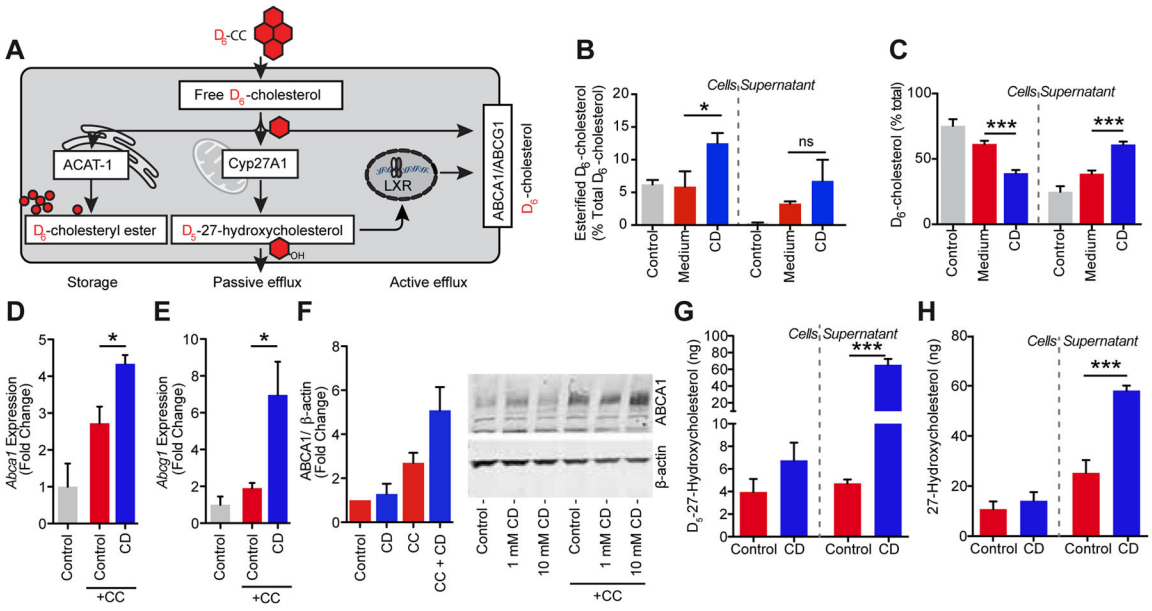

Fig. 4. CD mediates metabolism and efflux of crystal-derived cholesterol

(A) Macrophages loaded with CCs prepared from D_6-cholesterol (D_6-CC) can reduce the amount of free, crystal-derived D_6-cholesterol by three main mechanisms: First, acetyl-CoA acetyltransferase (ACAT1) can catalyze the formation of D_6-cholesteryl esters, the storage form of cholesterol which is deposited in lipid droplets. Second, the mitochondrial enzyme 27-hydroxylase (Cyp27A1) can catalyze the formation of D_5-27-hydroxycholesterol, which can passively diffuse across cell membranes. Third, D_5-27-hydroxycholesterol is a potent activator of LXR transcription factors, which in turn mediate the up-regulation of the cholesterol efflux transporters ABCA1 and ABCG1. **(B, C)** iMacs loaded with 200 μg D_6-CC/1×10^6 cells for 3 h were treated with 10 mM CD or vehicle control prior to GC-MS-SIM analysis of crystal-derived cholesterol. **(B)** Percentage of esterified D_6-cholesterol in cell and supernatant fractions before CD treatment (control bar) and upon 48 h CD treatment. **(C)** Efflux of D_6-cholesterol into supernatants of D_6-CC-loaded macrophages before CD treatment (control bar) and upon 24 h CD treatment. Gene expression of **(D)** *Abca1* and **(E)** *Abcg1*, and **(F)** protein expression of ABCA1 in BMDMs loaded with 100 μg CC/1×10^6 cells for 3 h followed by incubation with 10 mM CD or medium control for **(D, E)** 4 h or **(F)** 24 h. Immunoblot in **(F)** is representative of three independent experiments and densitometric analysis of all three experiments is provided for 10 mM CD and presented as ABCA1 expression relative to the loading control β-ACTIN. Data are shown as means + s.e.m. of at least three independent experiments. **(G)** D_5-27-hydroxycholesterol in cell and supernatant fractions of iMacs loaded with 200 μg D_6-CC/1×10^6 cells for 3 h prior to 48 h treatment with 10 mM CD or medium control determined by GC-MS-SIM. **(H)** 27-hydroxycholesterol in cell and supernatant fractions of iMacs upon 48 h treatment with 10 mM CD or medium control. **(B, C)** Medium vs. CD, unpaired two-tailed Student's t test; **(D–F)** CC+Control vs. CC+CD, unpaired two-tailed Student's t test; **(G, H)** Control vs. CD, unpaired two-tailed Student's t test; ***p < 0.001, *p < 0.05, ns = not significant.

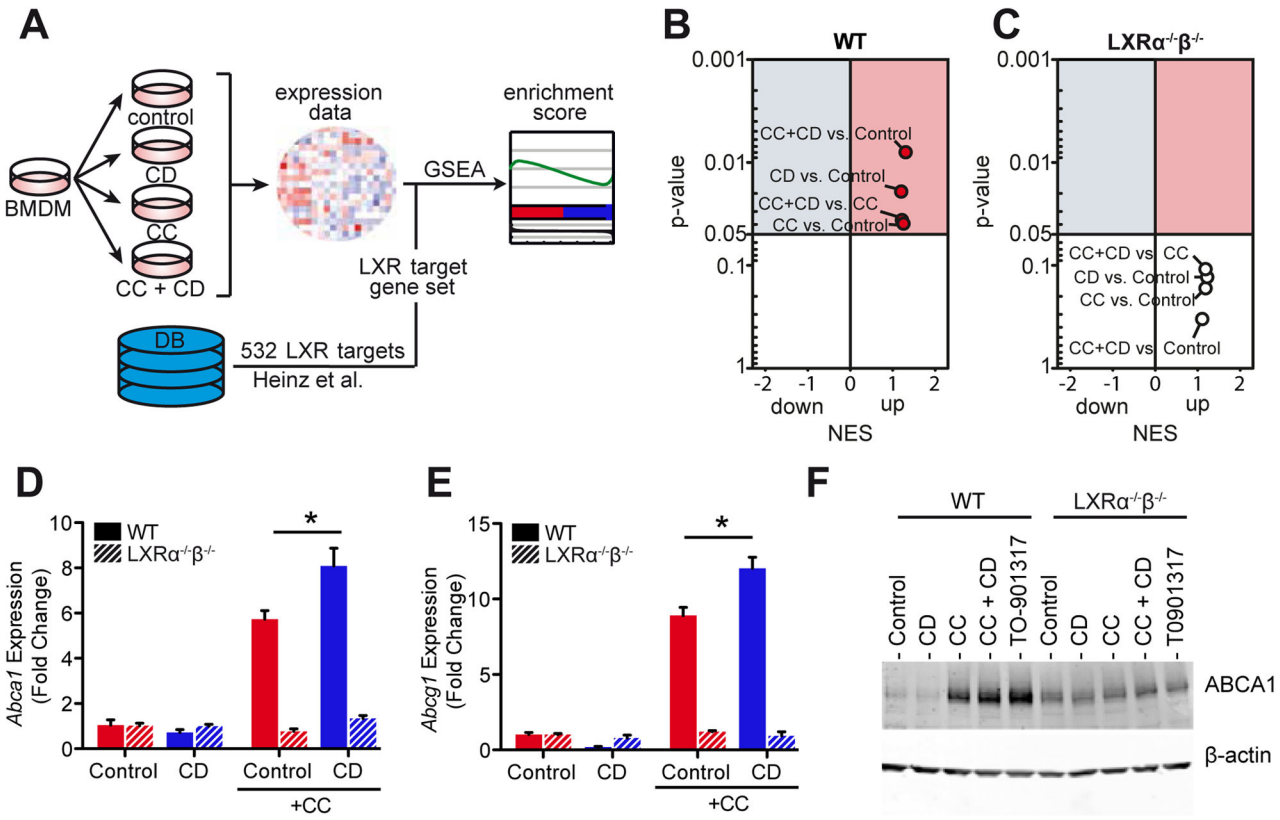

Fig. 5. CD induces LXR target gene expression in WT macrophages

(A) BMDMs from WT and LXRα$^{-/-}$β$^{-/-}$ mice loaded with 100 μg CC/1×10^6 cells for 3 h and incubated with 10 mM CD for 4 h for microarray analysis. GSEA for LXR target gene sets described in Heinz *et al.* (30) (Table S1) was performed on gene expression data. **(B, C)** GSEA results for **(B)** WT and **(C)** LXRα$^{-/-}$β$^{-/-}$ BMDMs presented as volcano plots of normalized enrichment score (NES) and enrichment p-values. Red circles show positively and significantly enriched gene sets (NES>1, p-value<0.05). **(D–F)** Gene expression of **(D)** *Abca1* and **(E)** *Abcg1*, and **(F)** protein expression of ABCA1 in BMDMs from WT and LXRα$^{-/-}$β$^{-/-}$ mice loaded with 100 μg CC/1×10^6 cells for 3h followed by incubation with 10 mM CD for **(D, E)** 4 h or **(F)** 24 h. The synthetic LXR agonist T0901317 (10 μM) was used as a positive control for ABCA1 protein induction. Immunoblot in **(F)** is representative of two independent experiments. Data are shown as mean + s.e.m. of two independent experiments. CC+Control vs. CC+CD, unpaired two-tailed Student's t test; *p < 0.05.

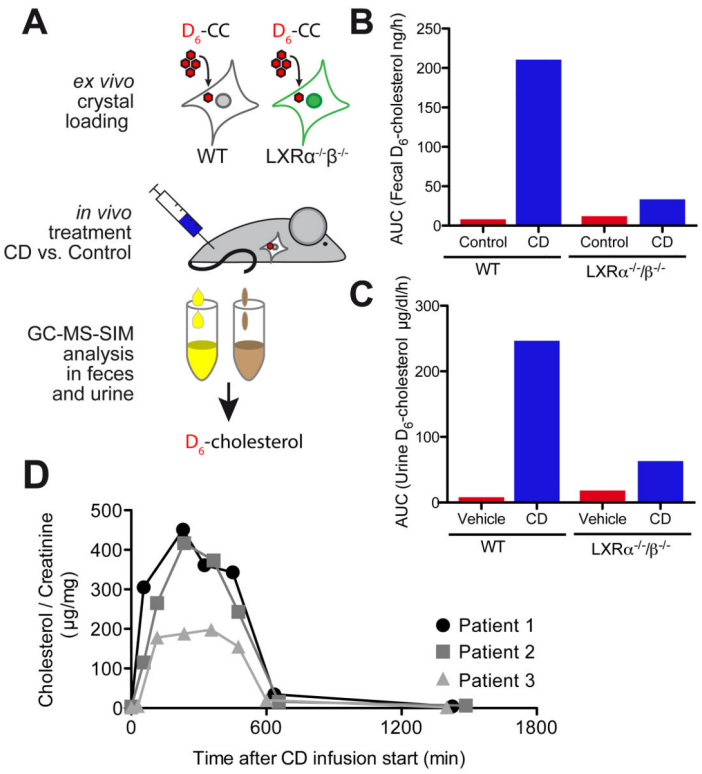

Fig. 6. CD facilitates RCT *in vivo* and promotes urinary cholesterol excretion

(A) BMDMs from WT or LXRα$^{-/-}$β$^{-/-}$ mice were loaded with 100 µg D_6-CC/1×10^6 cells and injected into the peritoneum of WT mice. Subsequently, mice were treated subcutaneously with 2 g CD/ kg body weight or vehicle control (n=4 per group). D_6-cholesterol content in **(B)** feces and **(C)** urine collected every 3 h over 30 h post CD injection. Data is shown as total area under the curve of excreted D_6-cholesterol pooled from the mice within a group per time point. **(D)** Urine samples collected from three individual NPC1 patients upon intravenous application of CD for specific treatment of NPC. Urine cholesterol concentration was determined by GC-MS-SIM and normalized to urine creatinine excretion.

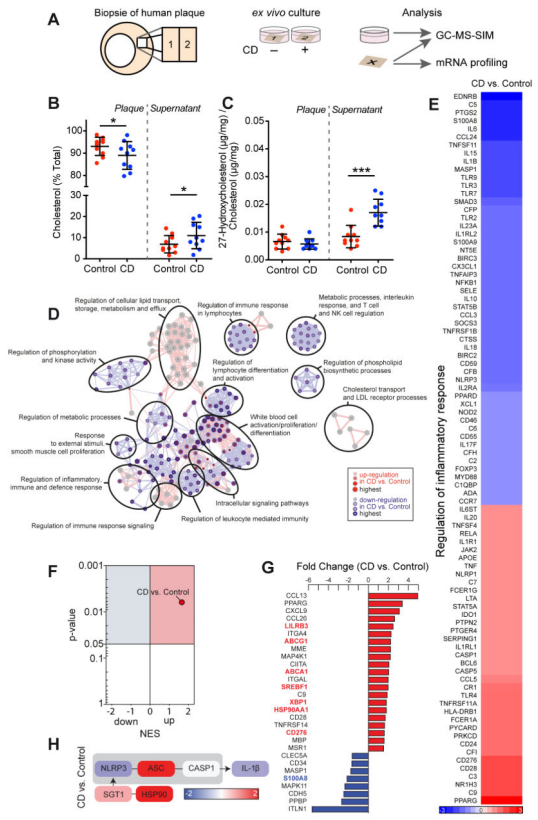

Fig. 7. CD induces cholesterol metabolism and an anti-inflammatory LXR profile in human atherosclerotic carotid plaques

(A) Human atherosclerotic carotid plaques obtained by carotid endarterectomies (n=10) were split into two macroscopically equal pieces and cultured for 24 h with 10 mM CD or control. Half of the plaque tissue was used for mRNA profiling with nCounter analysis system (Nanostring technologies), the other half and the culture supernatant were analyzed by GC-MS-SIM. **(B)** Cholesterol efflux from plaque tissue into supernatants displayed as % of total cholesterol per sample. **(C)** Distribution of 27-hydroxycholesterol relative to cholesterol in plaque and supernatant. **(D)** GOEA of differentially expressed (DE) genes (FC>1.3, p-value<0.05) visualized as GO network, where red nodes indicate GO term enrichment by up-regulated DE genes and blue borders indicate GO term enrichment by downregulated DE genes. Node size and border width represent the corresponding FDR-adjusted enrichment p value (q value). Edges represent the associations between two enriched GO terms based on shared genes, where edge thickness indicates the overlap of genes between neighbor nodes. Highly connected terms were grouped together and were annotated manually by a shared general term. **(E)** Heat map of genes involved in the GO term “Regulation of inflammatory response” (GO:0050727). Color bar indicates fold change. **(F)** Volcano plot of NES and enrichment p-values based on GSEA for the LXR target gene set (Table S3). Red circle indicates positively and significantly enrichment of the LXR target gene set (NES>1, p-value<0.05). **(G)** Top DE genes determined by 3-way ANOVA (FC>1.5, p-value<0.05). LXR target genes are colored in red or blue. **(H)** Gene expression of genes relevant for the NLRP3 inflammasome pathway. Color bar indicates

fold change. **(B, C)** Data are shown as mean +/− s.e.m. CD vs. Control, paired two-tailed Student's t test; ***p < 0.001, *p < 0.05.

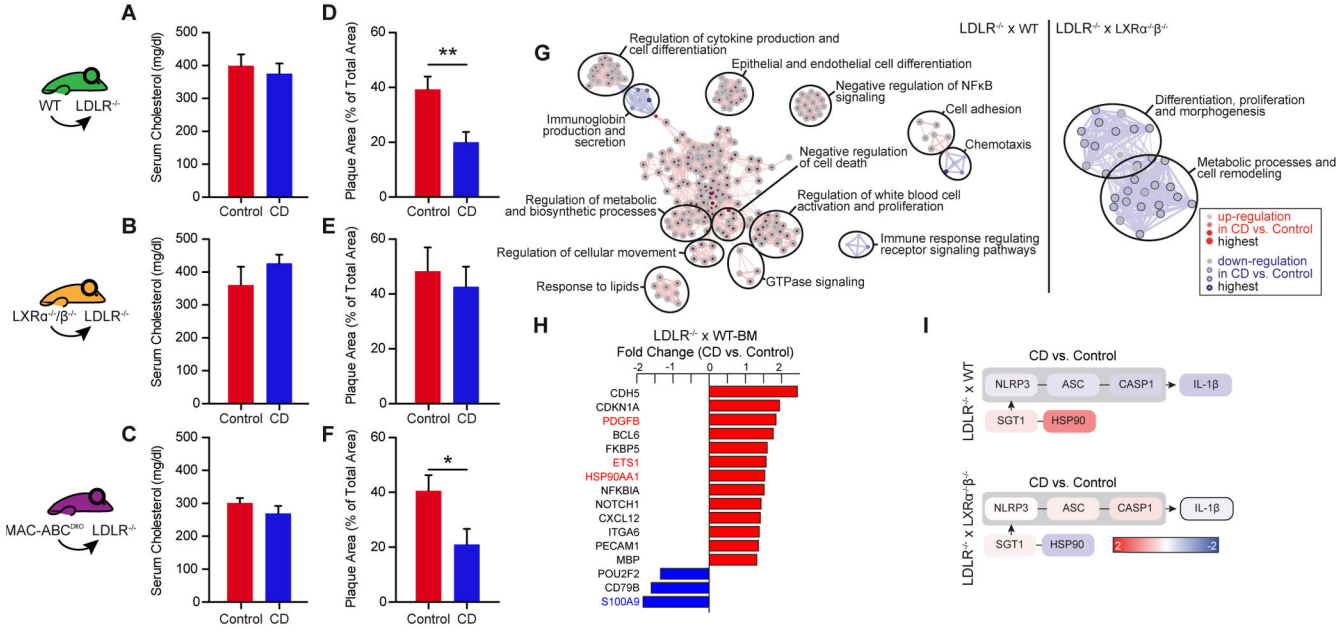

Fig. 8. CD impairs atherogenesis and regulates metabolic and anti-inflammatory processes in an LXR-dependent manner

LDLR$^{-/-}$ mice were transplanted with WT, LXRα$^{-/-}$β$^{-/-}$ or MAC-ABC^{DKO} bone marrow. They were then fed a cholesterol-rich diet for eight weeks and concomitantly treated with 2g CD/ kg body weight or vehicle control twice a week (n=6–8 per group). **(A–C)** Plasma cholesterol levels of CD- and vehicle-treated animals. **(D–F)** Atherosclerotic plaque area relative to total arterial wall area. **(G–I)** Descending aortas of LDLR$^{-/-}$ mice transplanted with WT and LXRα$^{-/-}$β$^{-/-}$ were used for gene expression analysis by microarray, with subsequent filtration for the genes included in the human plaque mRNA profiling. **(G)** GOEA of differentially expressed (DE) genes (FC>1.3, p-value<0.05) visualized as GO network, where red nodes indicate GO term enrichment by up-regulated DE genes and blue borders indicate GO term enrichment by downregulated DE genes. Node size and border width represent the corresponding FDR-adjusted enrichment p value (q value). Edges represent the associations between two enriched GO terms based on shared genes, where edge thickness indicates the overlap of genes between neighbor nodes. Highly connected terms were grouped together and were annotated manually by a shared general term. **(H)** DE genes determined by 3-way ANOVA (FC>1.3, p-value<0.05) in aortas of LDLR$^{-/-}$ mice transplanted with WT bone marrow. LXR target genes are colored in red or blue. **(I)** Gene expression of genes relevant for the NLRP3 inflammasome pathway. Color bar indicates fold change. **(A, B)** Data are shown as mean + s.e.m., CD vs. Control, unpaired two-tailed Student's t test; **p < 0.01, *p < 0.05.